1967-06

The Intertropical Convergence Zone and Vertical Motions Using A Diagnostic Numerical Model.

Murray, John Francis; Prokop, Phil George

Monterey, California. U.S. Naval Postgraduate School

THE INTERTROPICAL CONVERGENCE ZONE AND VERTICAL MOTIONS USING A DIAGNOSTIC NUMERICAL MODEL

PHIL GEORGE PROKOP
and
JOHN FRANCIS MURRAY

THE INTERTROPICAL CONVERGENCE ZONE AND VERTICAL MOTIONS USING A DIAGNOSTIC NUMERICAL MODEL

by

Phil George Prokop
Lieutenant Commander, United States Navy
B.A., San Diego State College, 1954

and

John Francis Murray
Lieutenant, United States Navy
B.A., Villanova University, 1959

Submitted in partial fulfillment of the
requirements for the degree of

MASTER OF SCIENCE IN METEOROLOGY

from the

NAVAL POSTGRADUATE SCHOOL
June 1967

ABSTRACT

A diagnostic, non-linear balanced model is applied to a case study in the tropical Western Pacific on 1 and 3 March 1965. The region includes both sides of the equator and contains the ITCZ.

A discussion of the ITCZ is given and the model is discussed along with the processing of the input data. The study contains the horizontal wind velocity and the thermal distribution as input values. The non-divergent stream function (ψ) is obtained by relaxation of the Poisson Equation, $\nabla^2\psi = k\cdot\nabla\times V = 3$, where the vorticity is computed from the observed wind field. A comparison is made between the non-divergent part of the wind and the actual wind. Computer analyzed stream functions at several levels are shown and discussed.

Dry adiabatic vertical velocities are obtained and compared with the ITCZ. Typical magnitudes are on the order of 0.5 cm/sec. The forcing functions of the ω equation are shown and the contributions, in partitioned form, by various terms are illustrated and discussed at several levels.

ERRATA

Title Page: Chairman, Department of Meteorology add and Oceanography

p. 24, par. 2, line 8 change effects to affects

p. 27, par 2 1), line 1 change sparce to sparse

p. 75, paragraph beginning Verticle structure, line 7 change overlaid to overlain

TABLE OF CONTENTS

LIST OF ILLUSTRATIONS

TABLE OF SYMBOLS AND ABBREVIATIONS

c_p	Coefficient of specific heat at constant pressure
f	Coriolis parameter
g	Acceleration of gravity
$\mathbb{K}$	Unit vector in the z-direction
p	Atmospheric pressure
R	Specific gas constant
σ	Static stability
T	Temperature
V_H	Horizontal velocity vector
Z	Height of the isobaric surfaces
α	Specific volume
β	Northward variation of Coriolis parameter
θ	Potential temperature
ϕ	Geopotential, gZ
χ	Velocity potential for the irrotational component of velocity
ψ	Stream function for the non-divergent component of velocity
ω	The individual change of pressure, dp/dt
∇	Isobaric gradient operator
∇^2	Laplacian operator
J	Jacobian operator
u	Zonal component of the wind
v	Meridional component of the wind
u_ψ	Zonal component of the non-divergent wind
v_ψ	Meridional component of the non-divergent wind
ζ	Relative Vorticity

ζ_a	Absolute vorticity
ρ	Density
C_D	Drag coefficient
H_S	Sensible heating function
H_L	Latent heating function
mb	Millibar
ITCZ	Intertropical Convergence Zone
neph	Nephanalysis
prog	Prognosis
π	$\frac{RT}{p\theta}$
τ_x	$C_D \rho u \sqrt{u^2+v^2}$
τ_y	$C_D \rho v \sqrt{u^2+v^2}$

I. INTRODUCTION

The tropical atmosphere has been the object of an intensive research effort in recent years. No single, dynamically consistant model has been developed which yields completely acceptable results, and although great progress has been made through computer application to case studies, some of the questions raised are still unanswered.

Lack of conventional data severly hinders analysis in any tropical study and it seems unlikely that a significant improvement in the number of reporting stations is forthcoming in the near future. The alternative for those interested in the problem is to rely more heavily on "unconventional" or satellite data, including photographs and radiation data, and possibly satellite tracking of constant level balloons. The Intertropical Convergence Zone(ITCZ) the Equatorial Trough, and the Intertropical Front have been used by various meteorologists to describe the same meteorological phenomena. A finer distinction could perhaps be made, but for the purpose of this paper ITCZ is preferred and will be defined as a relatively narrow, quasi-continuous band of convective clouds encircling the earth with associated synoptic scale vertical velocities caused by the convergence of air masses originating in the Trade Wind systems of both hemispheres. The other definitions will be used interchangeably when referring to the literature. The weather associated with this zone is often severe, convective in nature, and in the tropics exceeded only by hurricanes and typhoons.

A multi-level diagnostic non-linear balanced model is a useful tool in studying the three-dimensional structure of the atmosphere and such a model has been successfully used by Krishnamurti (1966) in tropical and mid-latitude studies. Charney (1963) argued that vertical motions in the tropics are small and may be neglected. Krishnamurti believes that even though small, they may play an important role in the dynamics of the tropics. He found typical values of vertical velocity on the order of 0.1 cm sec^{-1} in a typical Carribbean easterly wave and 1-2 cm sec^{-1} in the considerably more active Indian monsoon circulation which becomes part of the ITCZ during the northern summer. Together with the horizontal winds, the vertical velocity completely describes the three-dimensional motion of the atmosphere.

The authors applied the model used by Krishnamurti and Baumhefner, (1966) with some modifications, to a case study in the Western Pacific in order to obtain vertical velocities in the ITCZ. Other considerations motivating the work were, to investigate the non-divergent stream function derived from the relative vorticity field on and near the Equator, and to define initial state conditions for use in a more sophisticated model, such as a primitive equation prediction scheme as suggested by Charney, (1962).

A barotropic model is currently being used to forecast the non-divergent wind field and at present is pro-

ducing acceptable results. Once the data problem in the tropics is solved, however, the baroclinic terms will have to be included and a significant improvement should be realized.

History. Historically the ITCZ has been a frustrating and confusing phenomenon. Lacking a complete understanding of the major forces involved in the tropics, meteorologists of various schools attempted to apply their theories to the tropical problem. Palmer (1951) and Riehl (1954) divide the approaches into three broad categories: Climatological, Air Mass, and Perturbation. The Climatologists based their interpretation of the ITCZ on long term mean charts, statistical in nature, and based on a simple general circulation theory. The data network in the tropics may be sufficient for their purposes, however, they are unable to explain the large daily fluctuations and severe storms frequently found in the equatorial regions. The mean position of the equatorial trough, based on isobaric analysis, is shown in Fig. 1. The Scandinavians, who are primarily responsible for the air mass approach, applied their frontal theory to the tropics and the term Intertropical Front was coined. Indeed, the weather was of a frontal nature caused by the air masses of the two hemispheres converging in a low pressure trough, although a significant density discontinuity was not observed. The ITCZ was subsequently described by various authors as:

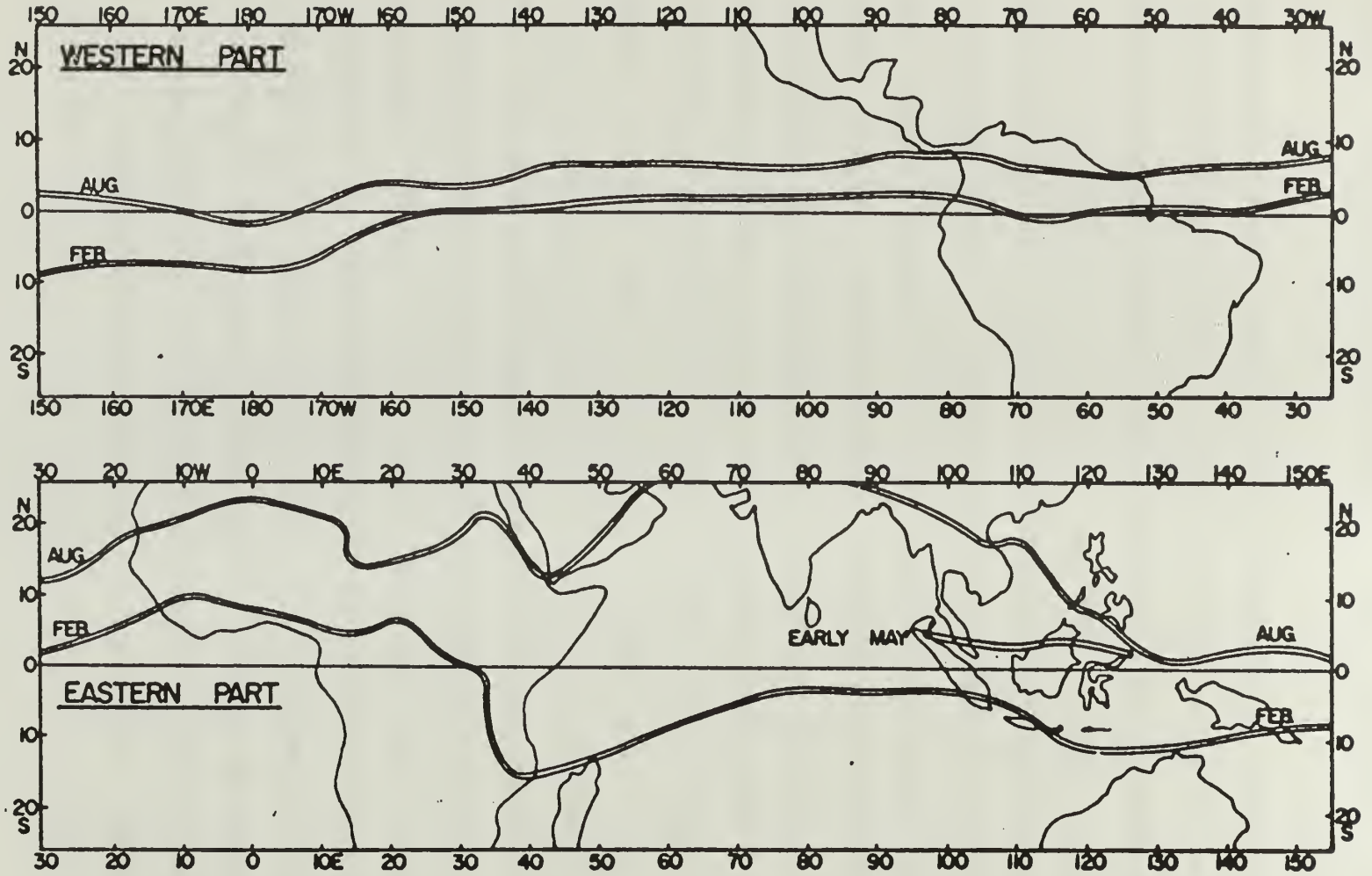

Fig. 1. Mean positions of the Equatorial trough in the IGY months of August 57 and February 58 and over Southeast Asia in early May.

1) a single and continous front
2) a double front
3) part single and part double fronts
4) discontinuous
5) sloping toward the summer hemisphere
6) sloping arbitrarily
7) not sloping at all
8) it moves discontinuously
9) it disappears at one location while another forms at a new location.

It is not surprising that this theory also failed the test in that it could not be used as a short term forecast aid. No dynamic explanation could be offered for the varied structure and movement of the front and the theory was abandoned.

Riehl (1954) describes Palmer's attempt to consolidate the previous work into a unified picture in the Perturbation approach theory. In a Pacific study he found that the East Central Pacific wind constancy is high and the equatorial trough has little variation. Small disturbances that perturb the flow are either brought into the area or develop there. They then move downstream as waves in the Equatorial Easterlies. Convergence in the basic flow tends to amplify cyclonic crests and dampen anticyclonic ones. If the axis of symmetry for the waves is on the equator, both northern and southern crests of the waves represent cyclonic

circulation and will intensify due to the convergent flow. This may lead to what has been termed a split or double equatorial trough. With continued amplification, closed circulations appear and a west wind finally appears at the equator. The result of a large number of these circulations near the equator becomes evident in a mean wind analysis showing a west component in very low latitudes. These west winds are shown by Wiederanders (1961) to appear only below 500 mbs. Originating in the trades, they cross the equator, recurve and form a westerly asymptote of convergence. This phenomena seems apparent in this study on 1 March.

The Perturbation approach, although a significant improvement over the Climatological and Frontal approach, was not wholly satisfactory and many of the dynamic problems are still with us.

II. DESCRIPTION OF THE MODEL

Dynamical multi-level models enable a study of vertical motions of a particular system or area. The concept of using balanced models for providing an initial state for primitive equation models was first proposed by Charney (1955). The balanced model initial state has the advantage of suppressing the unwanted gravitational instabilities that observed initial data might generate. In recent studies of tropical storms, balanced models have been proposed by Ooyama (1963), Charney (1963), Rosenthal (1964) and Kuo (1965).

A multi-level diagnostic balance model has been demonstrated to be a powerful tool for studying the three-dimensional details of the non-geostrophic behavior of the atmosphere during various stages of a storm development (Krishnamurti, Nogues and Baumhefner, 1966). Baumhefner (1966) used a similar model, but with additional terms, for a case study in the Caribbean. The model presented here is essentially the same as that used by Baumhefner, but with minor modifications in calculating the non-divergent stream function and using actual observed temperatures, as suggested by him.

It must be kept in mind that there is actually a two-fold purpose involved with the use of this model. One is diagnostic, and the second, and more far reaching, is that these results are to be used in the future in a multi-level primitive equation prediction scheme as input data.

The balance model provides a synoptic scale vertical motion field which is determined by numerical calculation on a horizontal mesh whose size is a few degrees of latitude. The numerical model selected to describe the three-dimensional structure of the tropics is commonly called the non-linear, or multi-level balanced model (Charney, 1962). Baroclinic vertical motions of a complete balanced model can be partitioned to determine the unique contributions of several forcing functions. These may be looked on as several synoptic mechanisms producing ascending or descending motions.

A formal derivation of this model has been done by Baumhefner (1966), and further explanations are contained in Krishnamurti (1966b). Therefore, this work will not be repeated here, other than to give the final form of the omega equation of a general balance model and to point out the alternate method that was used to calculate the non-divergent stream function.

The ω-equation of a general balanced model is expressed by the following three equations for ω, χ, and $\frac{\partial \psi}{\partial t}$.

$$\begin{aligned}\nabla^2\sigma\omega + f^2\frac{\partial^2\omega}{\partial p^2} = {} & f\frac{\partial}{\partial p}J(\psi, \mathcal{S}_a) + \pi\nabla^2 J(\psi,\theta) \\ & -2\frac{\partial}{\partial t}\frac{\partial}{\partial p}J\left(\frac{\partial\psi}{\partial x},\frac{\partial\psi}{\partial y}\right) - f\frac{\partial}{\partial p}(\mathcal{S}\nabla^2\chi) \\ & + f\frac{\partial}{\partial p}g\frac{\partial}{\partial p}\left[\frac{\partial\tau_y}{\partial x} - \frac{\partial\tau_x}{\partial y}\right] - \frac{R}{c_p p}\nabla^2 H_L \\ & - \frac{R}{c_p p}\nabla^2 H_s + f\frac{\partial}{\partial p}\left\{\omega\frac{\partial}{\partial p}\nabla^2\psi\right\} \\ & + f\frac{\partial}{\partial p}\left\{\nabla\omega\cdot\nabla\frac{\partial\psi}{\partial p}\right\} - f\frac{\partial}{\partial p}\{\nabla\chi\cdot\nabla\mathcal{S}_a\} \\ & - \pi\nabla^2\{\nabla\chi\cdot\nabla\theta\} - \beta\frac{\partial}{\partial p}\frac{\partial}{\partial y}\frac{\partial\psi}{\partial t} \end{aligned} \tag{1}$$

$$\nabla^2\chi = \frac{\partial\omega}{\partial p} \tag{2}$$

$$\nabla^2 \frac{\partial \psi}{\partial t} = -J(\psi, S_a) - g \frac{\partial}{\partial p}\left[\frac{\partial \tau_y}{\partial x} - \frac{\partial \tau_x}{\partial y}\right] + \nabla\chi \cdot \nabla S_a + S_a \nabla^2 \chi - \nabla\omega \cdot \nabla \frac{\partial \psi}{\partial p} - \omega \frac{\partial}{\partial p} \nabla^2 \psi. \qquad (3)$$

These equations are solved by numerical techniques.

The general balance ω-equation, presented here, has 12 forcing functions.

The forcing functions are:

1. $f \frac{\partial}{\partial p} J(\psi, S_a)$ — Differential vorticity advection by the non-divergent part of the wind.
2. $\pi \nabla^2 J(\psi, \theta)$ — Laplacian of thermal advection by the non-divergent part of the wind.
3. $-2 \frac{\partial}{\partial t} \frac{\partial}{\partial p} J\left(\frac{\partial \psi}{\partial x}, \frac{\partial \psi}{\partial y}\right)$ — Differential deformation effect.
4. $-f \frac{\partial}{\partial p} (S \nabla^2 \chi)$ — Differential divergence effects of a balance model.
5. $f \frac{\partial}{\partial p} g \frac{\partial}{\partial p}\left[\frac{\partial \tau_y}{\partial x} - \frac{\partial \tau_x}{\partial y}\right]$ — Effects of frictional stresses.
6. $-\frac{R}{c_p p} \nabla^2 H_L$ — Effects of latent heat.
7. $-\frac{R}{c_p p} \nabla^2 H_S$ — Effects of sensible heat transfer from water surfaces to the atmosphere.
8. $f \frac{\partial}{\partial p}\left\{\omega \frac{\partial}{\partial p} \nabla^2 \psi\right\}$ — Differential vertical advection of vorticity.
9. $f \frac{\partial}{\partial p}\left\{\nabla\omega \cdot \nabla \frac{\partial \psi}{\partial p}\right\}$ — Differential turning of vortex tubes.
10. $-f \frac{\partial}{\partial p}\left\{\nabla\chi \cdot \nabla S_a\right\}$ — Differential advection of vorticity by the divergent part of the wind.
11. $-\pi \nabla^2\left\{\nabla\chi \cdot \nabla\theta\right\}$ — Laplacian of thermal advection by the divergent part of the wind.

12. $-\beta \frac{\partial}{\partial p} \frac{\partial}{\partial y} \frac{\partial \Psi}{\partial t}$ Contribution by the beta term of the vorticity equation.

It should be noted here that, in this form, none of the terms "blow up" at the equator where the Coriolis parameter (f) goes to zero. Instead, the forcing function just drops out. Zero values are not found in the output, however, due to the form of the relaxation process.

Calculations of the input values to solve our equations are, for the most part, pretty straightforward. Five point schemes are used for the Laplacian, the Liebmann forward extrapolation technique of relaxation is used, Jacobians are of the standard form and all derivatives are evaluated over distances $2\Delta x$ and $2\Delta y$. The following equations are pertinent.

Potential temperature: $$\theta = T\left(\frac{1000}{p}\right)^{R/c_p} \qquad (4)$$

Dry static stability: $$\sigma = -\frac{RT}{p\theta}\frac{\partial \theta}{\partial p} \qquad (5)$$

Absolute vorticity: $$S_a = \frac{\partial v}{\partial x} - \frac{\partial u}{\partial y} + f \qquad (6)$$

Since an analysis of the geopotential height field is not easily possible in the tropics, the so-called balance equation (7), which is a simplification of the divergence equation, was not used.

$$\nabla \cdot f \nabla \psi = \nabla^2 \phi - 2J\left(\frac{\partial \Psi}{\partial x}, \frac{\partial \Psi}{\partial y}\right) \qquad (7)$$

If the balance equation is used, the procedure is to find the non-divergent stream function (Ψ) from the geopotential height. The stream function is then used to find the vorticity.

The procedure was reversed, somewhat, in this paper. The method used to compute the non-divergent stream function is the procedure suggested by Thompson (1961), which begins with a field of isotachs and isogons. The Helmholtz equation is manipulated to form the equation:

$$\zeta = \left(\frac{\partial v}{\partial x} - \frac{\partial u}{\partial y}\right) = \nabla^2 \psi \qquad (8)$$

By relaxing the field of the vorticity for suitable boundary conditions, the non-divergent stream function on an isobaric surface is obtained.

The numerical method and boundary conditions for solving this equation are those given by Hawkins and Rosenthal (1965). The boundary values of the non-divergent stream function are made a function of the divergence of the wind, instead of the zero condition imposed on the solution by the balance equation. The values depend on the derivative of the velocity potential ($\frac{\partial \chi}{\partial n}$) ($n$ normal to the boundary, increasing outward). The boundary values of $\frac{\partial \chi}{\partial n}$ needed are calculated from an initial χ-field obtained from the solution of

$$\nabla^2 \chi = \nabla \cdot \mathbf{V}, \quad \chi = 0 \text{ on the boundary} \qquad (9)$$

where $\nabla \cdot \mathbf{V}$ is the divergence calculated from the wind analysis.

The non-divergent stream function calculated by this method is what Baumhefner (1966) calls the kinematic stream function, and is the method that he felt was most accurate in the tropics.

The numerical model accepts data at five levels (1000, 800, 600, 400, and 200 mbs.) and utilizes the X, Y, P coordinate system. The basic inputs are, the observed temperatures, and the isogons and isotachs of the actual wind at each level. The basic grid consists of 33 x 15 x 5 points along the zonal, meridional and vertical directions. Actual grid values are inscribed at 27 grid points in the zonal direction, but an artificial cyclical continuity is provided by extending the grid over 6 extra points by fitting a polynomial through the boundary conditions. This region is a numerical waste-box in the diagnostic studies but will become essential in the future prediction phase.

A vertical staggering of the grid was used as recommended by Krishnamurti (1966a), and the values of Ψ, χ and ζ appear at 1000, 800, 600, 400 and 200 mbs while $\theta, T, \sigma, \omega$, and $\frac{\partial}{\partial p}\frac{\partial \Psi}{\partial t}$ appear at 900, 700, 500, and 300 mbs. Other boundary conditions are, $\omega = \chi = (\frac{\partial}{\partial p}\frac{\partial \Psi}{\partial t}) = 0$ at the northern and southern wall. Boundaries are eliminated in the zonal direction by the use of the 6 additional points. ω is taken to be zero at the surface and at the top of our atmosphere, 100 mbs.

The wind velocity is used to obtain the vorticity, and, from the vorticity, the stream function is derived. The static stability is calculated from the temperature. These terms, together with a frictional effect from the streamlines, will yield the first approximation of the vertical motion.

The omega equation, used for the first approximation, does not contain any terms that are a function of omega. The first guess of the vertical motion is then used to calculate the non-linear terms containing omega. The latent heat term is added at this point, since it is non-linear in nature. An iterative process is performed until the difference between successive approximations is considered small.

A brief recapitulation of the general form and effect of the main forcing functions is warranted. A complete discussion of all terms is included in Krishnamurti, Nogues, and Baumhefner (1966) and Krishnamurti (1966b).

Basically, if the forcing function, F_i, is greater than zero, then in that region we can expect rising motions. There are exceptions to this rule, but generally this is true. Near the centers of maximum rising or sinking motions, F_i and ω_i have been found to be inversely proportional to each other (Krishnamurti, Nogues, and Baumhefner, 1966).

Baumhefner (1966) has shown that the four main contributing forcing functions in the tropics are terms 1, 2, 5, and 6 (page 19). The first two terms are the simplest to interpret. The effect of differential vorticity advection (term 1) is that if in the upper air there is a region of strong positive vorticity advection by the non-divergent component of the wind, then F_1 is greater than zero and rising motions would be found. The inverse holds for sinking motions. The Laplacian of thermal advection (term 2) has the effect, that at centers where warm air

advection is a maximum by the non-divergent component of the wind, F_2 is greater than zero and again rising motions will be found. The inverse again holds.

The other two terms, friction and latent heat, are of great significance in the tropics and are explained in great detail by both Krishnamurti (1966b) and Baumhefner (1966). Generally, F_5 (friction) will contribute rising motions in regions of cyclonic relative vorticity and sinking motions in regions of anticyclonic relative vorticity. This effect will only be felt significantly at the 900 mb output level. A drag coefficient (C_D) of 2.0×10^{-3} was used, and held constant in the horizontal.

The latent heat term (term 5) contributes in the tropics where the following conditions are met:

1. The atmosphere is conditionally unstable.
2. Net moisture convergence in vertical columns is greater than zero.
3. The relative humidity at the particular level is greater than or equal to 60 percent.

This term only effects levels above 900 mbs, as that level is used as the top of the boundary layer. It is apparent that the latent heat term will have its greatest contribution to the rising motions where cumulus clouds are present.

III. RESEARCH PROCEDURES AND PROBLEMS

Initially, an attempt was made to produce a comprehensive, five day analysis covering the major portion of the Pacific from 40°N to 40°S. Plotted, mercator, 1:40,000,000 charts were obtained from the Hawaii Institute of Geophysics, University of Hawaii for 1 through 5 March 1965. Map time is 00Z. This period was chosen to allow a comparison of our results with those of Smagorinsky, whose report will be published at a later date. Since hand analysis had to be employed to prepare the input data, time considerations became a limiting factor and case studies on 1 and 3 March were agreed upon. The model employed in this study contains 27 grid points in the zonal direction and 15 points in the meridional direction spaced 2 degrees apart. This grid was placed in the area of most dense data in the Western Pacific where the analysis was felt to be most reliable and a well defined, if rather large, ITCZ was observed on the nephanalysis. The grid is bounded by the 128°E and 180° meridians and the 14°N and 14°S parallels. The area includes approximately 5.1 million square miles and contains sixteen reporting stations (Fig.2). Eleven of these are Radiosonde stations and 5 are Pibal stations, which report upper winds only.

Streamline, isotach, and temperature analyses were prepared for the 1000, 850, 700, 500, 300, and 200 mb levels, as well as a surface pressure analysis.

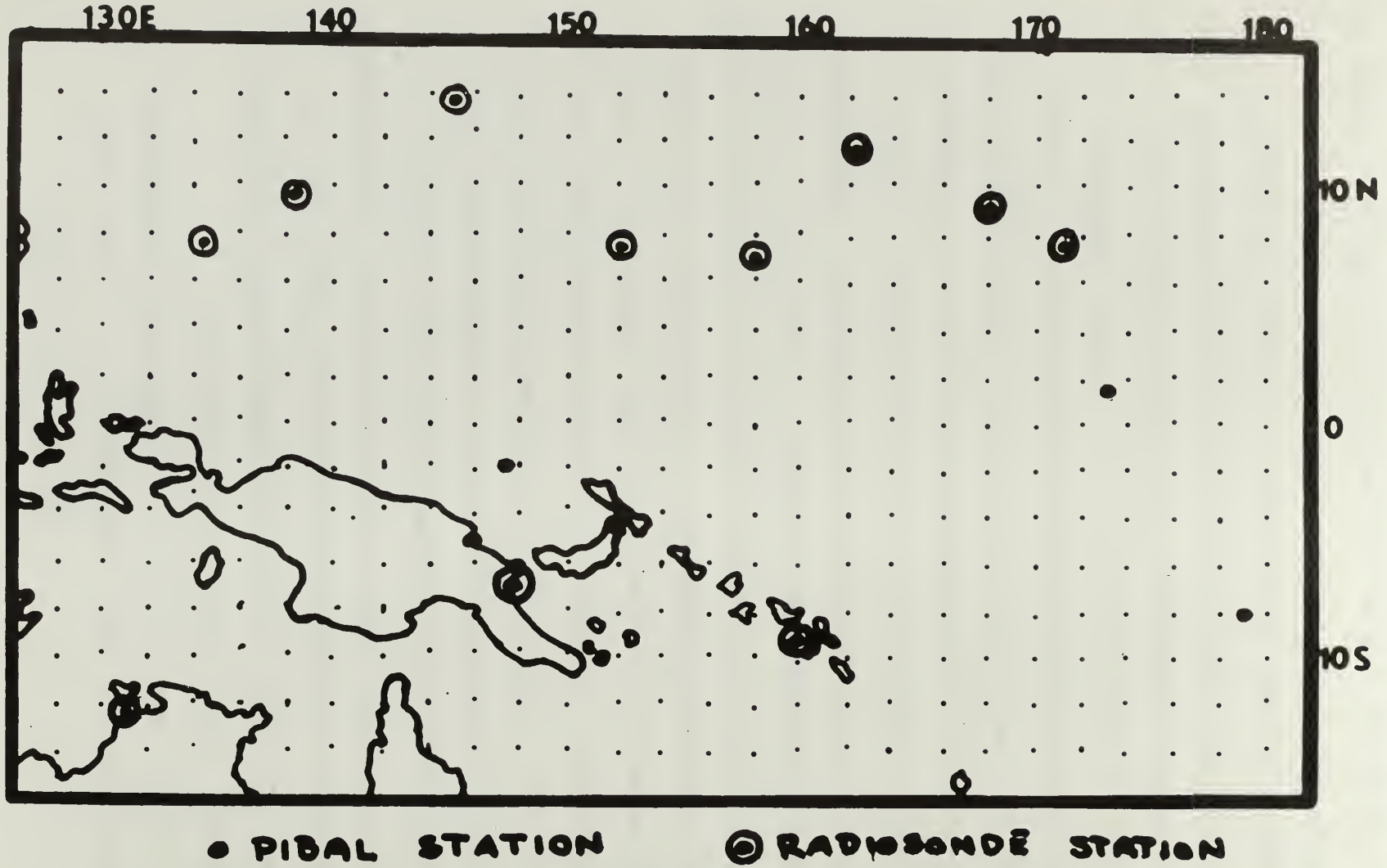

Fig. 2. Locations of the radiosonde and pibal stations used in the data analysis.

Isogon values were extrapolated to grid points using a parallel motion protractor and tabulated to 1 degree accuracy. Isotachs were analyzed at 5 knot intervals and extrapolated to tenths of knots. Temperatures were analyzed to whole degrees Centigrade and tabulated to tenths of degrees at grid points. Surface pressures were analyzed at one millibar intervals and tabulated to tenths of millibars.

A preliminary moisture analysis was prepared but was not satisfactory for our purposes and is not included in this study. The reason for its omission was based on two considerations:

1) The data was too sparce, and unreliable values were felt to have been generated at grid points between reporting stations.
2) The nephanalysis revealed only the gross features of the moisture field. A subjective scheme was considered, whereby typical relative humidities would be assigned to cloudy areas, and the moisture constructed from the humidities, however, lacking actual cloud photographs this method was also considered likely to result in inadequate gradients in both the horizontal and vertical.

The omission is a deficiency of this study since the release of latent heat is a major contributor to the vertical velocities in the tropics. The influence of terrain is also neglected.

Large vertical velocities can be obtained through orographic triggering mechanisms which would otherwise be unexplained dynamically.

Tiros IX negatives were obtained from NWRF Ashville, for the period 1 through 5 March 1965, but no useable frames were observed covering the area of interest during the days analyzed. Nephanalyses were constructed from the Tiros IX catalog, and original facsimile nephs, scaled to the computer output grid size. Channel two, 8-12 microns, Radiation Data was obtained from Goddard Space flight Center and was analyzed for March 3rd.

A minimum amount of subjectivity was employed in each of the analyses. The nephs were used as an aid in sparce data areas to locate major centers or regions of convergence. Wiederanders' Analysis of Monthly Mean Resultant Winds over the Pacific was also employed as a consistancy check. No reports were eliminated and gradients were extrapolated linearly in all fields. A few aircraft reports at non-standard levels were available and used if they could be extrapolated to the standard level without significantly altering the basic analysis. Vertical space or time cross-sections to eliminate or smooth erroneous data were not constructed due to time and data limitations.

The observed height fields were not analyzed for inclusion in this report in a smooth form. Rough sketches of these were prepared by the authors to compare with the geopotential heights constructed by the computer, on the basis

of input temperatures. The geopotential surfaces did not agree well with either the observed heights or the winds. Moreover, a continuous degradation was noted with increasing height. Baumhefner attempted to correct this in his study by subjectively modifying the geopotential heights to fit the observed winds, although weak temperature gradients may have been altered significantly. He remarked that using the observed, unadjusted geopotential heights to calculate thickness may lead to a more reliable calculation of temperatures. The authors, however, did not attempt this experiment, although it appears worthy of investigation.

To insure a smooth vertical temperature structure, successive averaging was accomplished, which resulted in the output temperatures varying slightly from input values.

Since the machine accepts data at the even levels mentioned previously, several techniques were employed to convert the data at the standard levels to the input levels within the computer. All data at the surface and 200 mb levels were used without modification. The temperature at 850 mbs was reduced to the 800 mb value, using a tropical, standard atmosphere lapse rate. The 600 and 400 mb levels were obtained using the mean of the 700 - 500 and 500-300 mb levels, respectively. The same scheme was used for wind data except that the wind vectors were separated into u and v components prior to averaging. The 850 mb winds were used directly as the 800 mb values.

A vertical staggering of the grid is convenient due to the nature of the hydrostatic and ω equations. The first part of the program, which does not include vertical velocities, yields outputs consisting of, temperature, potential temperature and static stability at the 900, 700, 500, and 300 mb levels. Geopotential heights, the stream function, and absolute vorticity appear at the 1000, 800, 600, 400, and 200 mb levels. The ω portion of the program provides vertical velocities at the 900, 700, 500, and 300 mb levels and we assume $\omega = 0$ at the surface and 100 mbs which represents the top of our atmosphere. The contributions to the total ω by various forcing functions are obtained, which allow an examination of their effects in the tropics. The sensible heat term contributed nothing in this study since we assumed thermal equilibrium between the atmosphere and ocean in the tropics. A discussion of the output charts is made in Chapter IV. The program was solved on an IBM 7094 computer and takes approximately one hour per case study.

IV. CASE STUDIES

0000Z 1 MARCH 1965

Synoptic situation. The most significant features in the surface pressure pattern on 1 March 1965, (Fig.3), are the low pressure center located in North Central Australia, and the trough extending from the Southern Hemisphere mid-latitudes to the equator. Two small high pressure centers are located in the Southern Hemisphere, one over New Guinea, and a second at 180° longitude. A secondary zonal trough is evident at 4°N extending from 145°E to 180°. The surface streamline pattern (Fig.5) agrees well with the pressure field. The winds are cyclonic around the Australian low with strong cyclonic shear and curvature, and the winds are anticyclonic around the high centered at 180°. The trough, which has been labeled Frontal on the nephanalysis, does not show up clearly in the wind field, but this is an area of very light winds and only a few reports were available. An asymptote of convergence is located in the zonal trough in the Northern Hemisphere. The winds to the north are extremely steady in direction but strong anticyclonic shear exists north of the isotach maximum at 6°N 164°E. A cyclonic eddy exists at 148°E just north of the equator. Equatorial Westerlies are formed as the N.E. Trades cross the equator and recurve west of 150°E under the influence of a change in sign of the Coriolis force. A split ITCZ forms. The nephanalysis (Fig.4) depicts, in the eastern section (orbit 456), the clouds associated with the frontal

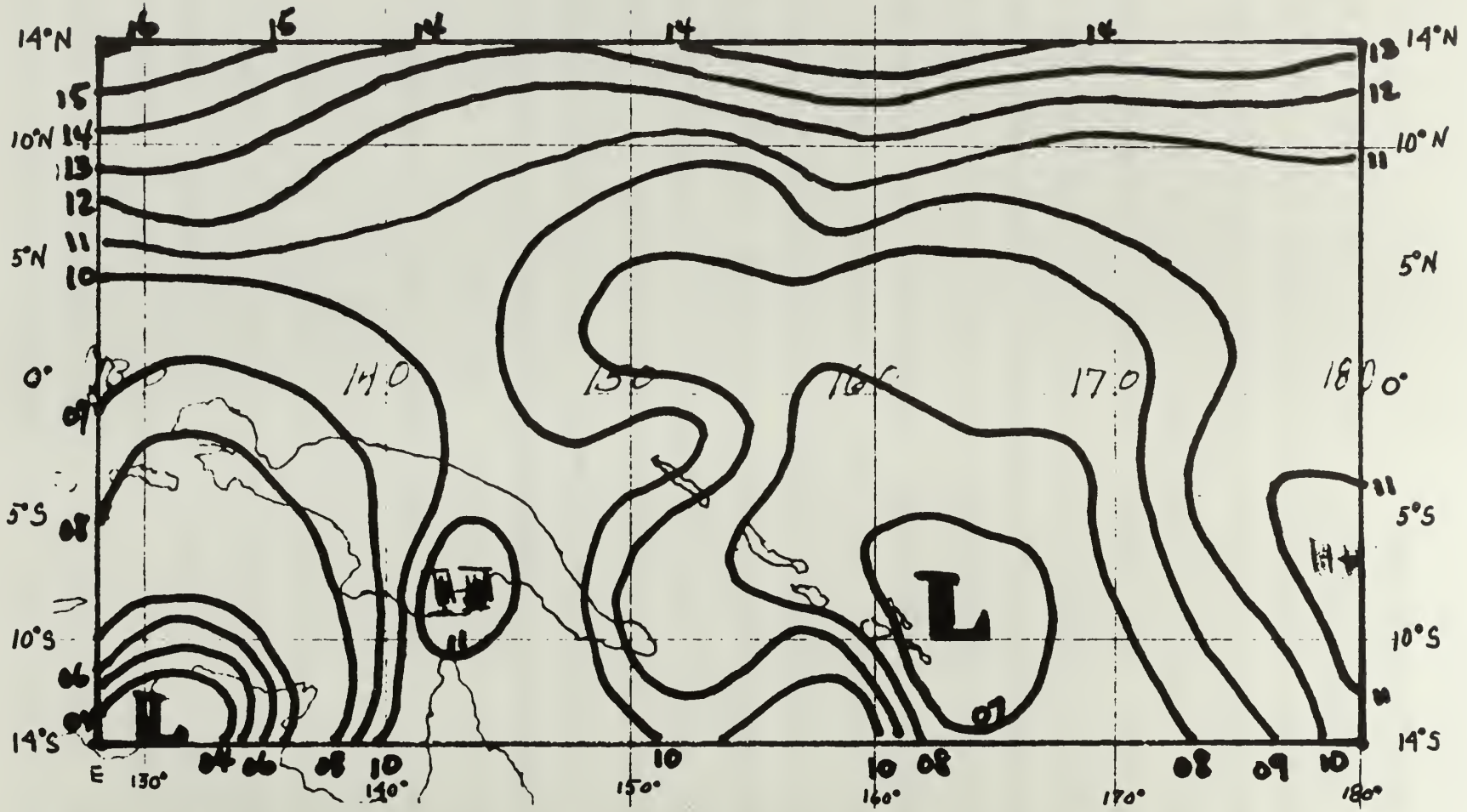

Fig. 3. Surface pressure, 00Z 1 March 1965.

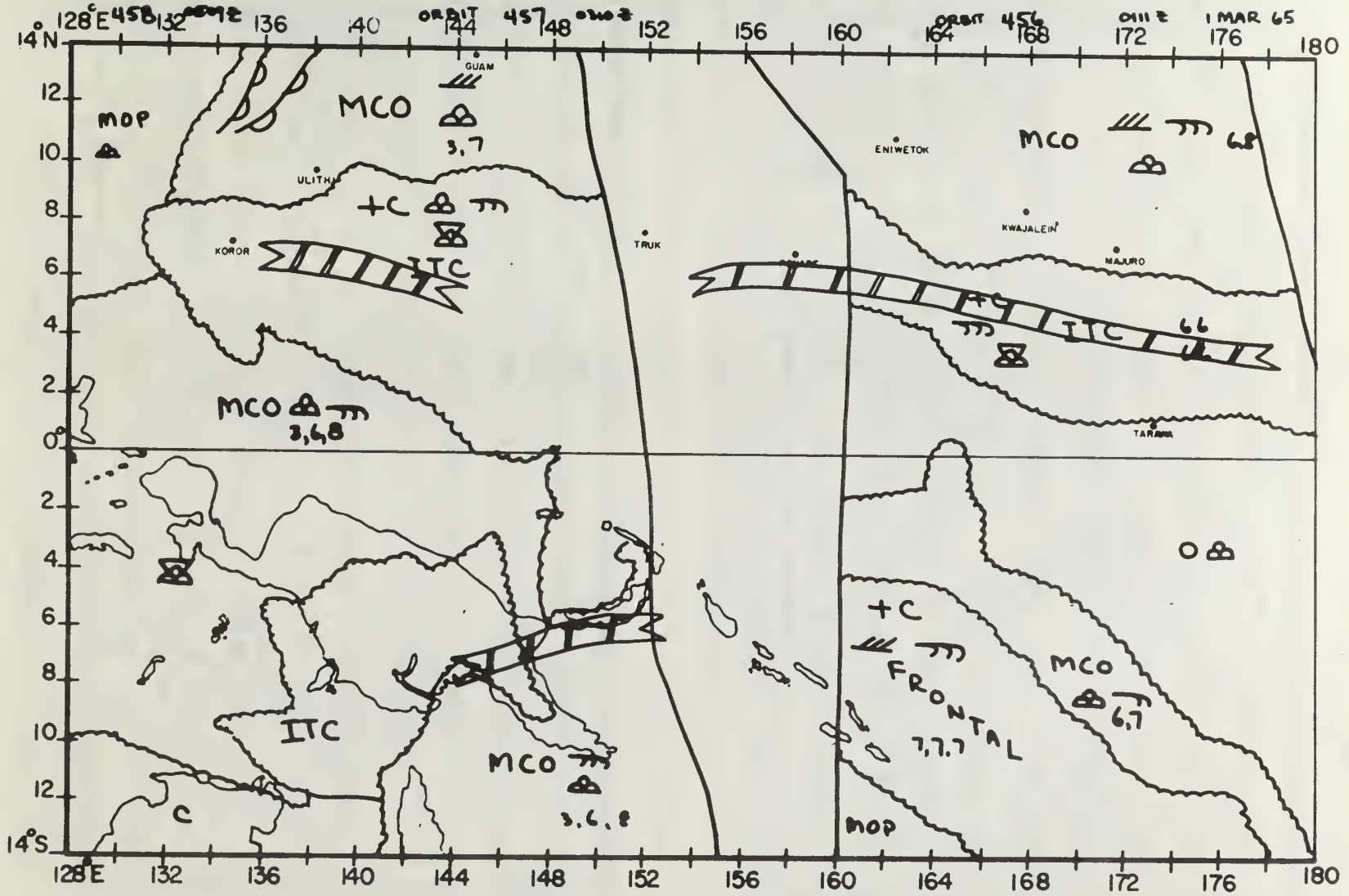

Fig. 4. Nephanalysis, 1 March 1965.

trough, an open area to the east and an ITC band located in the Northern Hemisphere in the area occupied by the zonal trough. The ITCZ is displaced far north of its mean position, which is at 8° South in February and early March. The western portion of the neph, orbits 457 and 458, shows most of the entire grid covered by clouds. The mostly open area, less than 5/10 coverage, in the northwest corner, is the result of a small high pressure ridge extending southward from higher latitudes. The ITCZ is an extremely wide band and is split into a northern and southern part. The southern band is not easily explained by the pressure field and we suspect a large terrain influence in this region. The 850 and 700 mb flow patterns (Fig. 6,7) are similar in most respects to the surface. At 500 mbs (Fig.9) the eddy which appeared north of the equator disappears and a large convergence area is found at 140°E 7°North. The Australian cyclone is still evident but the influence of the subtropical high pressure belts is becoming more apparent. At 300 and 200 mbs (Figs.9,10) these belts are the dominating features. More variability is noted at 200 mbs than at 300 mbs.

The observed temperature structure is very complex and appears to have little vertical continuity. Strong gradients may exist in localized areas which were not picked up in the analysis. The 850 and 200 mb temperatures are shown (Figs. 11,12) and they clearly show a reversal in the temperature gradient in the vicinity of the ITCZ. This feature was discovered by Schnapauff in the Atlantic and verified by

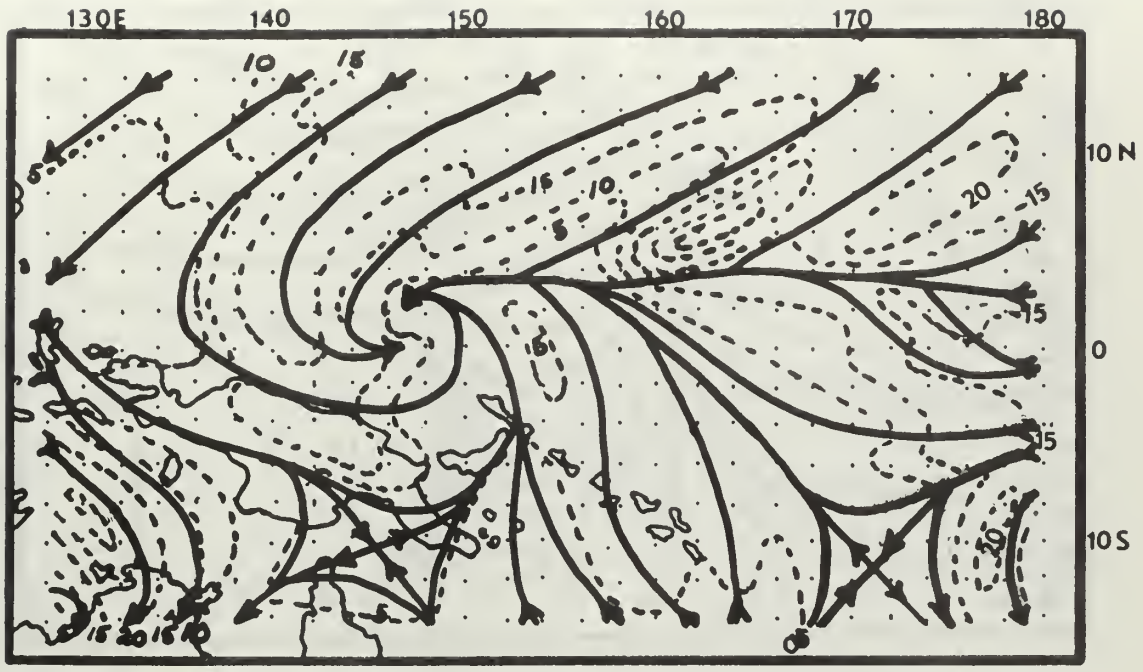

Fig. 5. Streamlines and isotachs at 1000 mbs, 00Z 1 March 1965. Isotach interval, 5 knots.

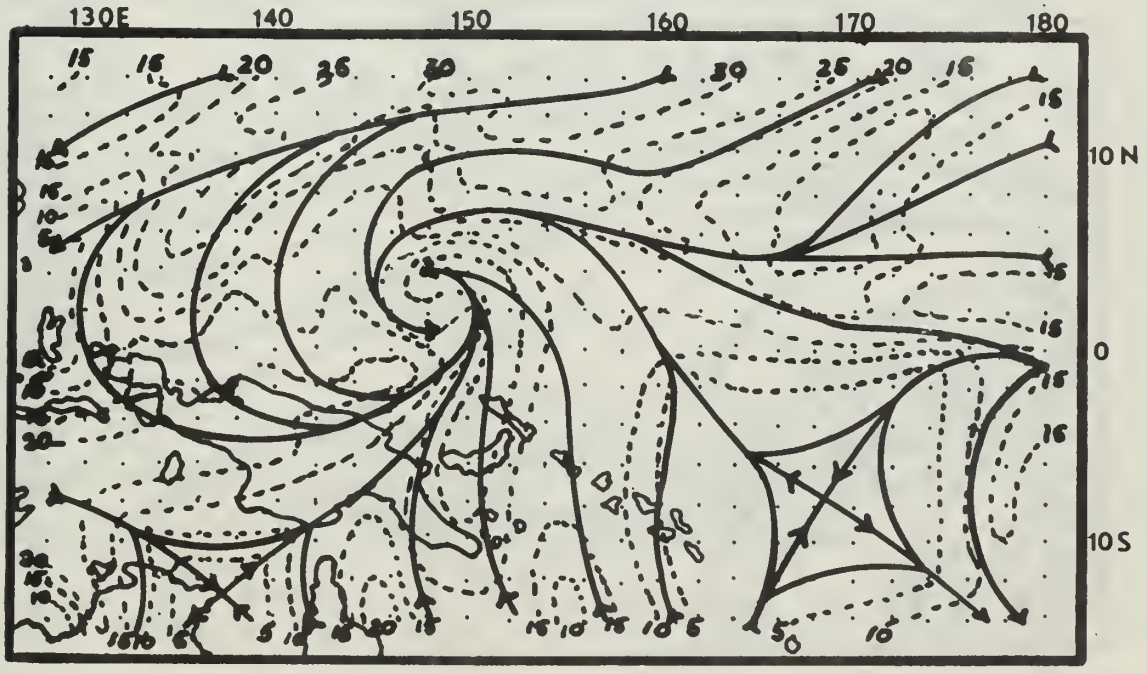

Fig. 6. Streamlines and isotachs at 850 mbs, 00Z 1 March 1965. Isotach interval, 5 knots.

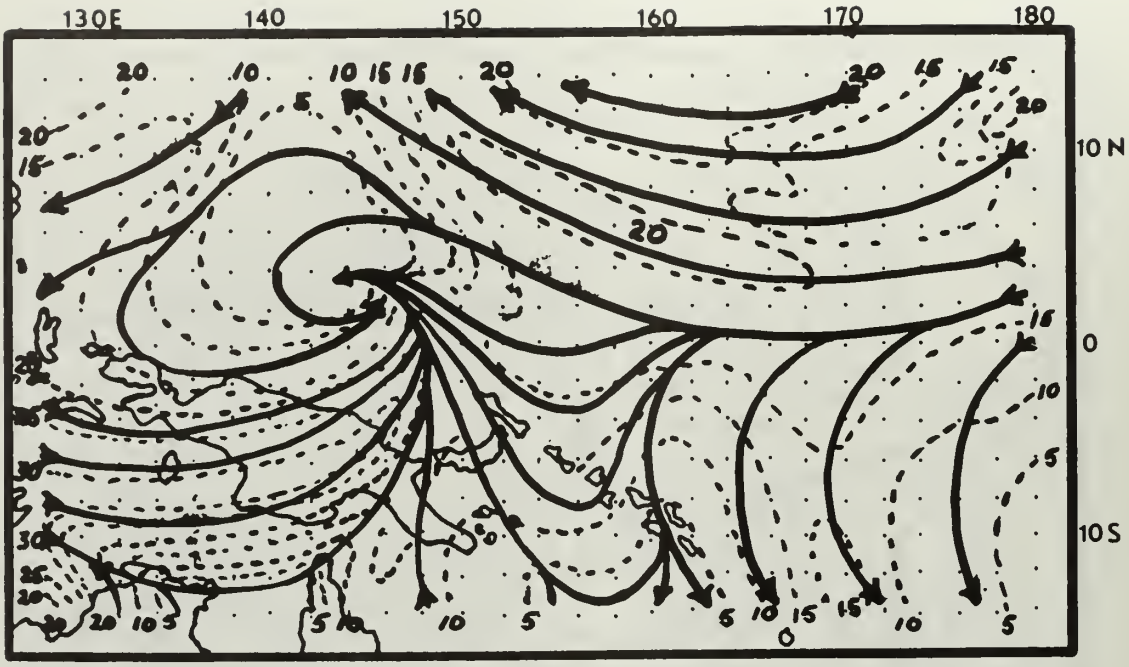

Fig. 7. Streamlines and isotachs at 700 mbs, 00Z 1 March 1965. Isotach interval, 5 knots.

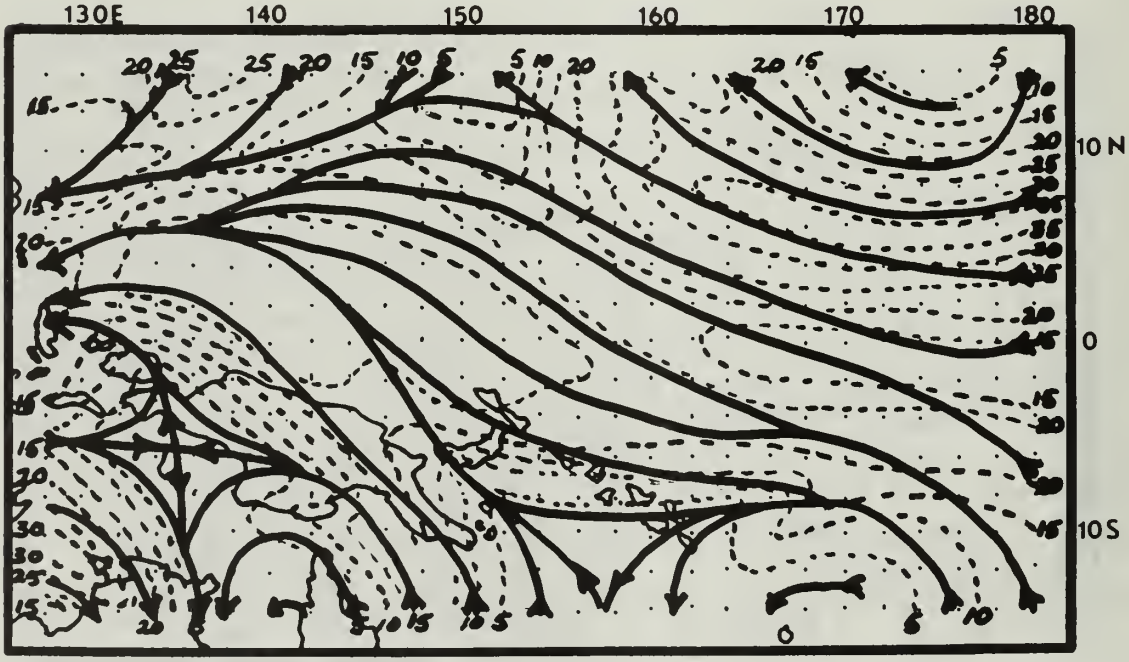

Fig. 8. Streamlines and isotachs at 500 mbs, 00Z 1 March 1965. Isotach interval, 5 knots.

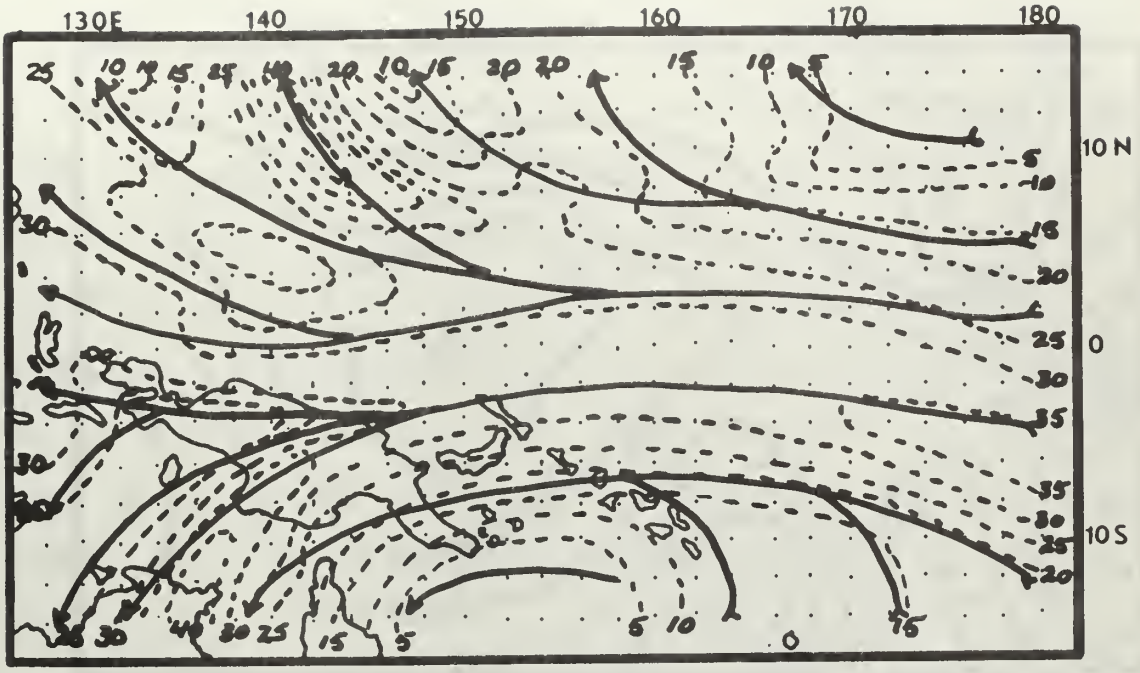

Fig. 9. Streamlines and isotachs at 300 mbs, 00Z 1 March 1965. Isotach interval, 5 knots.

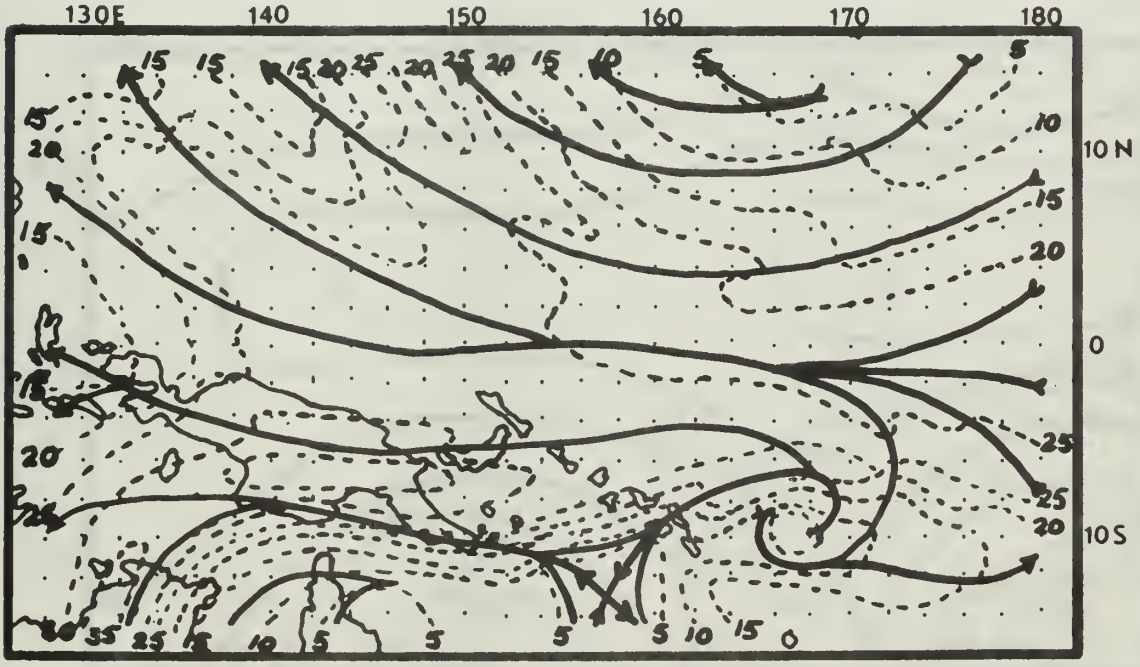

Fig. 10. Streamlines and isotachs at 200 mbs, 00Z 1 March 1965. Isotach interval, 5 knots.

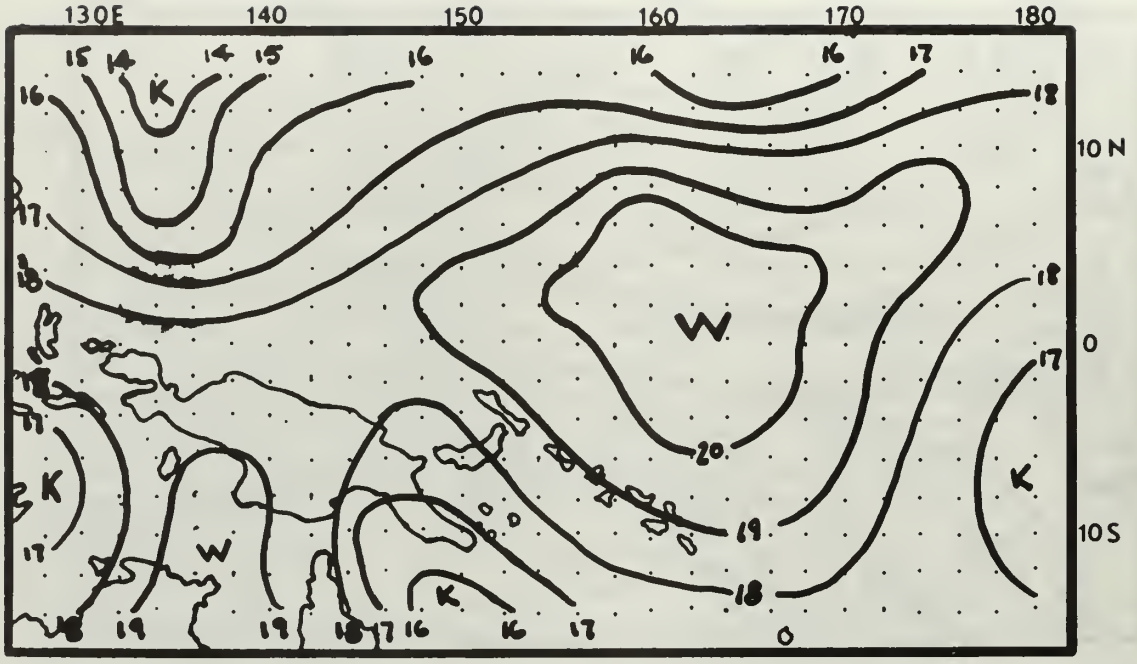

Fig. 11. Temperature analysis at 850 mbs, 00Z 1 March 1965. Temp. in degrees Centigrade. Isotherm interval, 1 degree.

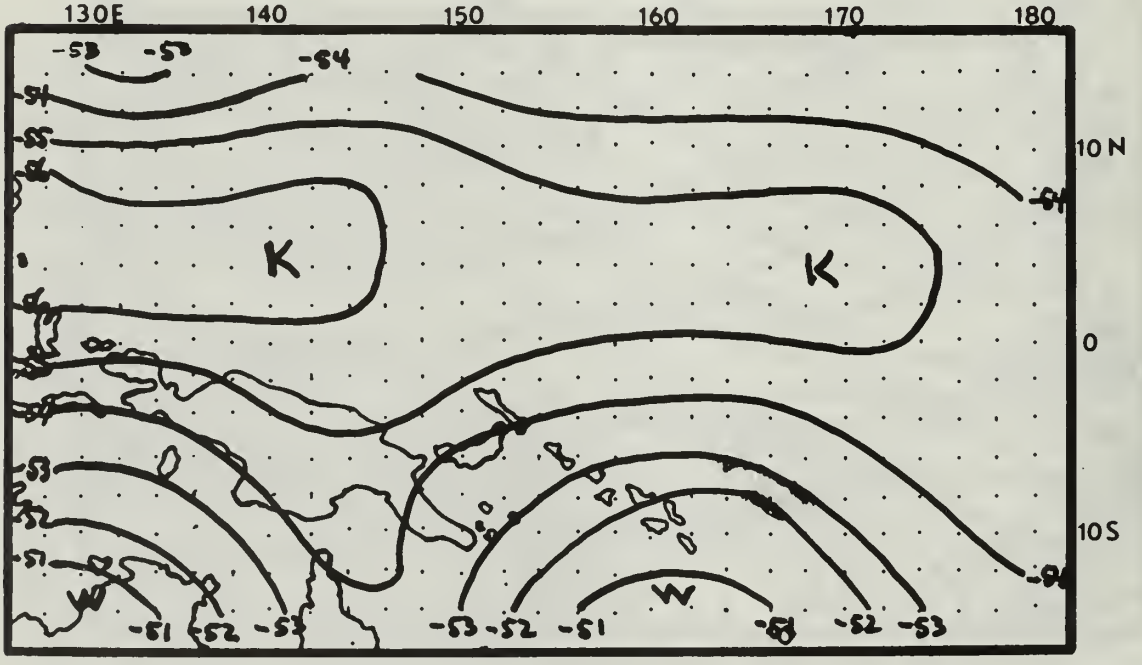

Fig. 12. Temperature analysis at 200 mbs, 00Z 1 March 1965. Temp. in degrees Centigrade. Isotherm interval, 1 degree.

Simpson in the Pacific. Riehl(1958)prepared a vertical cross-section of the typical temperature in the region of the equatorial trough, which is included for comparison (Fig.13a). Riehl also prepared a vertical cross-section of heights for this region (Fig.13b), and a comparison may be made with geopotential heights computed in the program from the surface pressure and vertical temperature structure. The 1000 mb geopotential height field (Fig.14) is shown as an example.

An example of the absolute vorticity, computed from the observed wind field, is shown for the 1000 mb level (Fig.15).

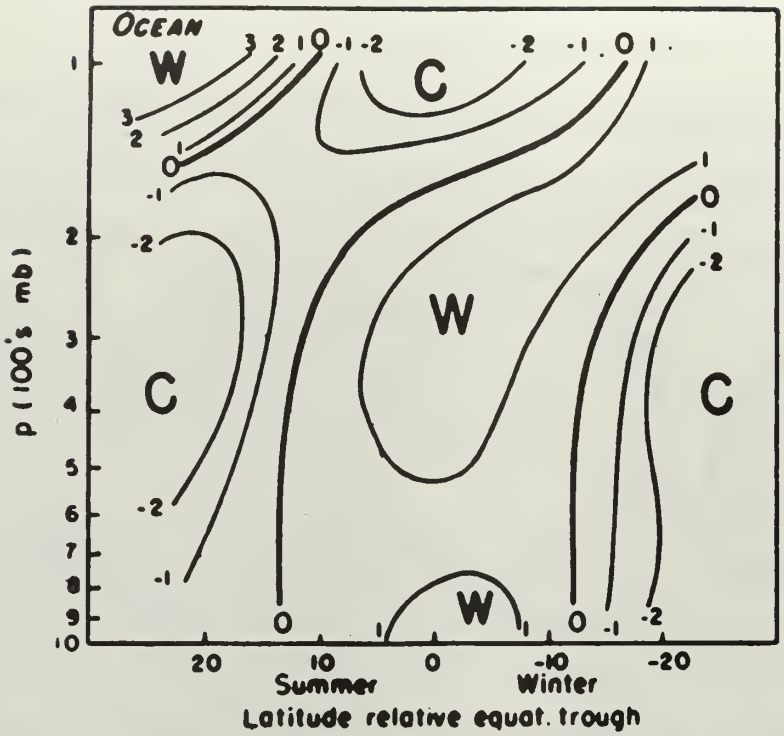

Fig. 13a. Vertical cross-section of temperature departure (°C) from horizontal mean, relative to equatorial trough, ocean areas.

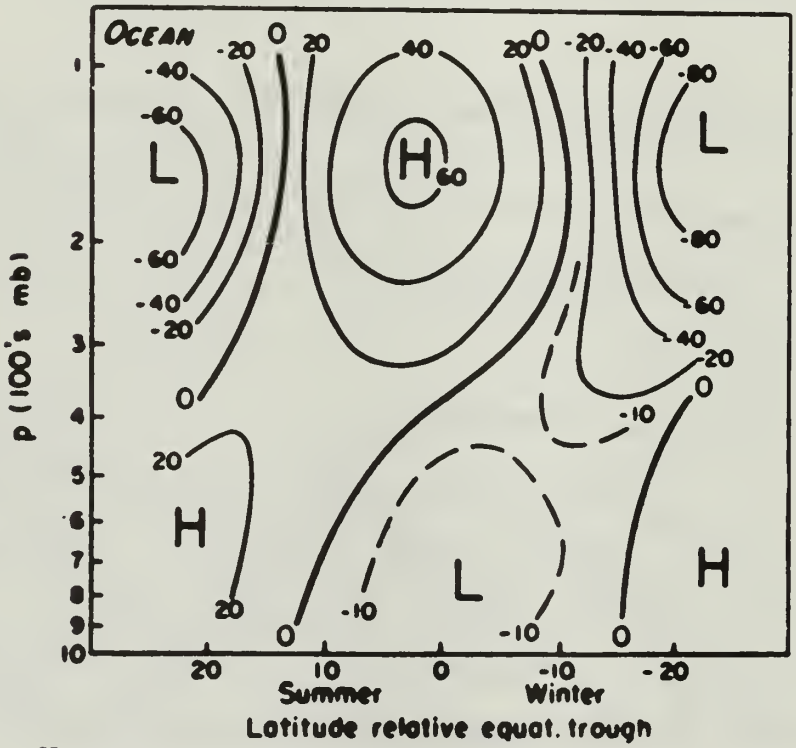

Fig 13b. Vertical cross-section of departure of height of isobaric surfaces (tens of feet) from horizontal means.

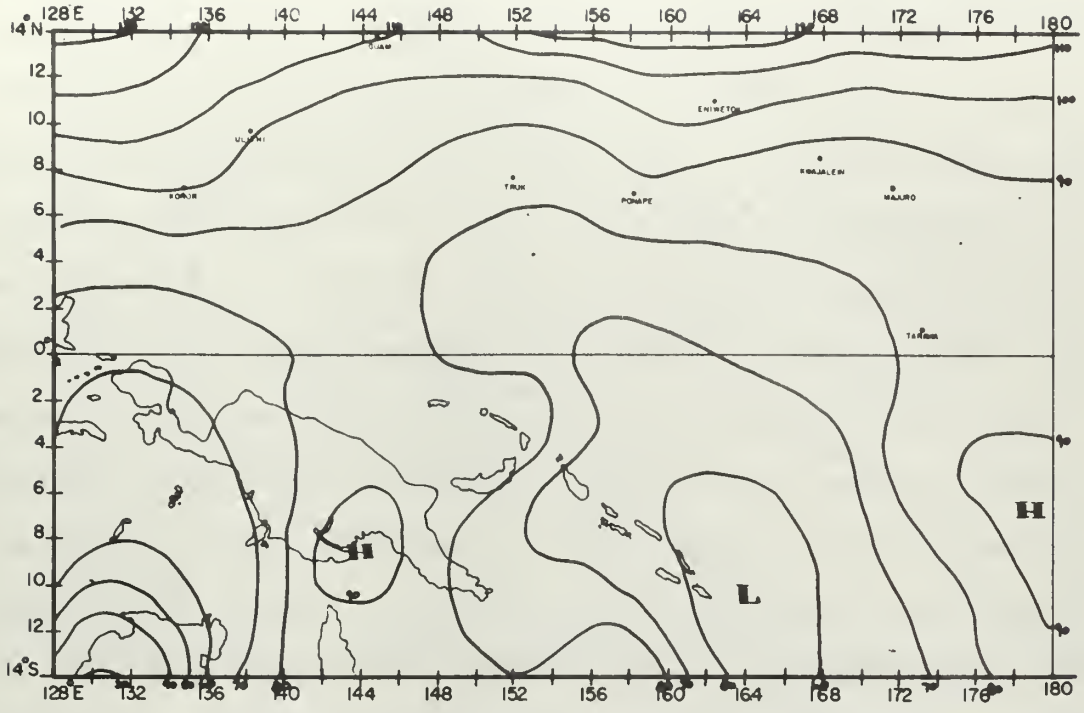

Fig. 14. Geopotential height at 1000 mbs, 00Z 1 March 1965. Heights in meters. Interval, 10 meters.

Fig. 15. Absolute vorticity at 1000 mbs, 00Z 1 March 1965. Interval 10 x 10^{-6} sec^{-1}.

Results. The results obtained through the application of this model to our study are most encouraging, particularly in the Northern Hemisphere where better data coverage was available. The stream functions generated through the relaxation of the vorticity field at 800 and 200 mbs are shown for 1 March in Figures 16 and 17. A comparison was made of the non-divergent wind and the actual winds in a meridional cross-section. At 800 mbs, only the u component of the actual wind is used since the cross section passed through the circulation center at 148°E, and the directions were more variable at this level. At 200 mbs, the longitude was chosen so that the streamlines had their maximum zonal values, and here, the total isotach value was used. These are plotted against the zonal stream wind u_ψ and are shown in Figure 18.

Baumhefner (1966) found that the non-divergent part of the wind was about 90% of the total wind and his results are clearly verified. Stream functions at the other levels yielded similar results.

Dry adiabatic vertical velocities are shown at the 900, 700, 500, and 300 mb levels,(Fig.19-22). An ITCZ was drawn in the areas of maximum rising motion on these charts such that it remained within the boundaries of the ITCZ indicated on the nephanalysis and at the same time was vertically consistent. The Northern Hemisphere fit was remarkable.

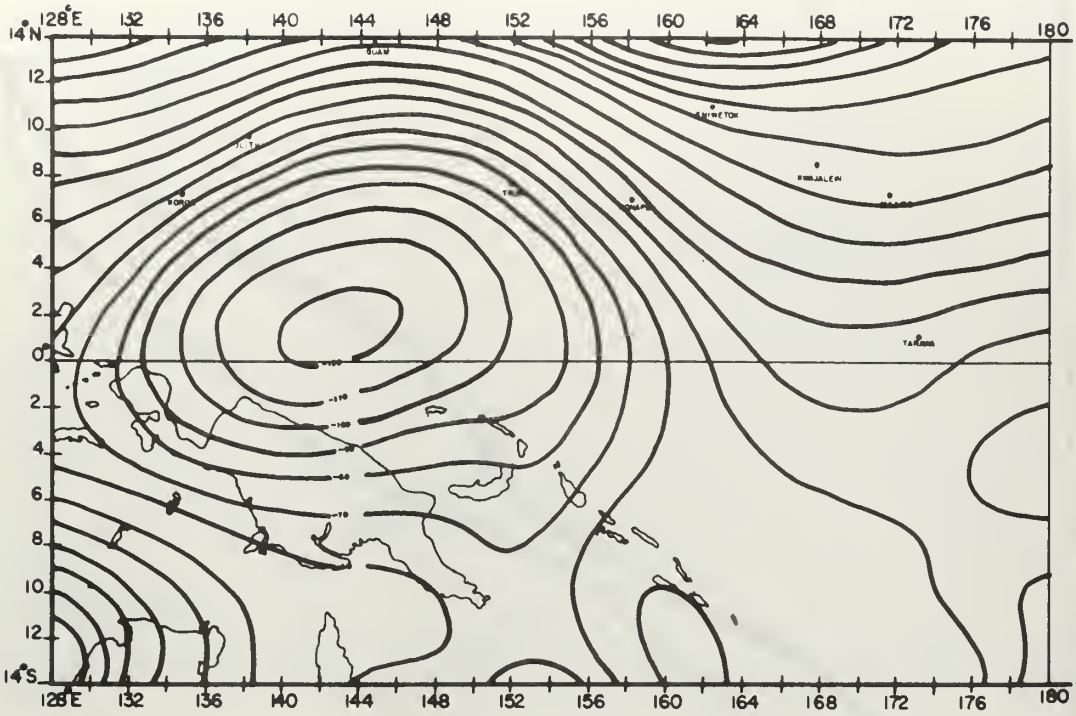

Fig. 16. Non-divergent stream function at 800 mbs, 00Z 1 March 1965. Isoline interval, 10×10^{-5} $m^2 sec^{-1}$.

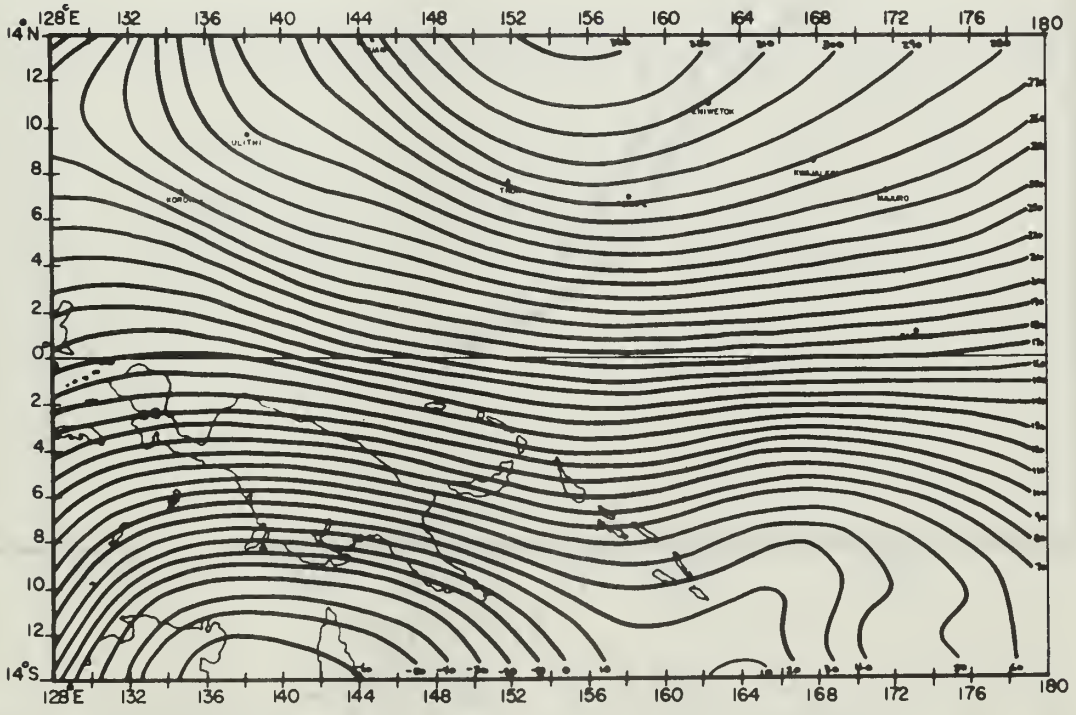

Fig. 17. Non-divergent stream function at 200 mbs, 00Z 1 March 1965. Isoline interval, 10×10^{-5} $m^2 sec^{-1}$.

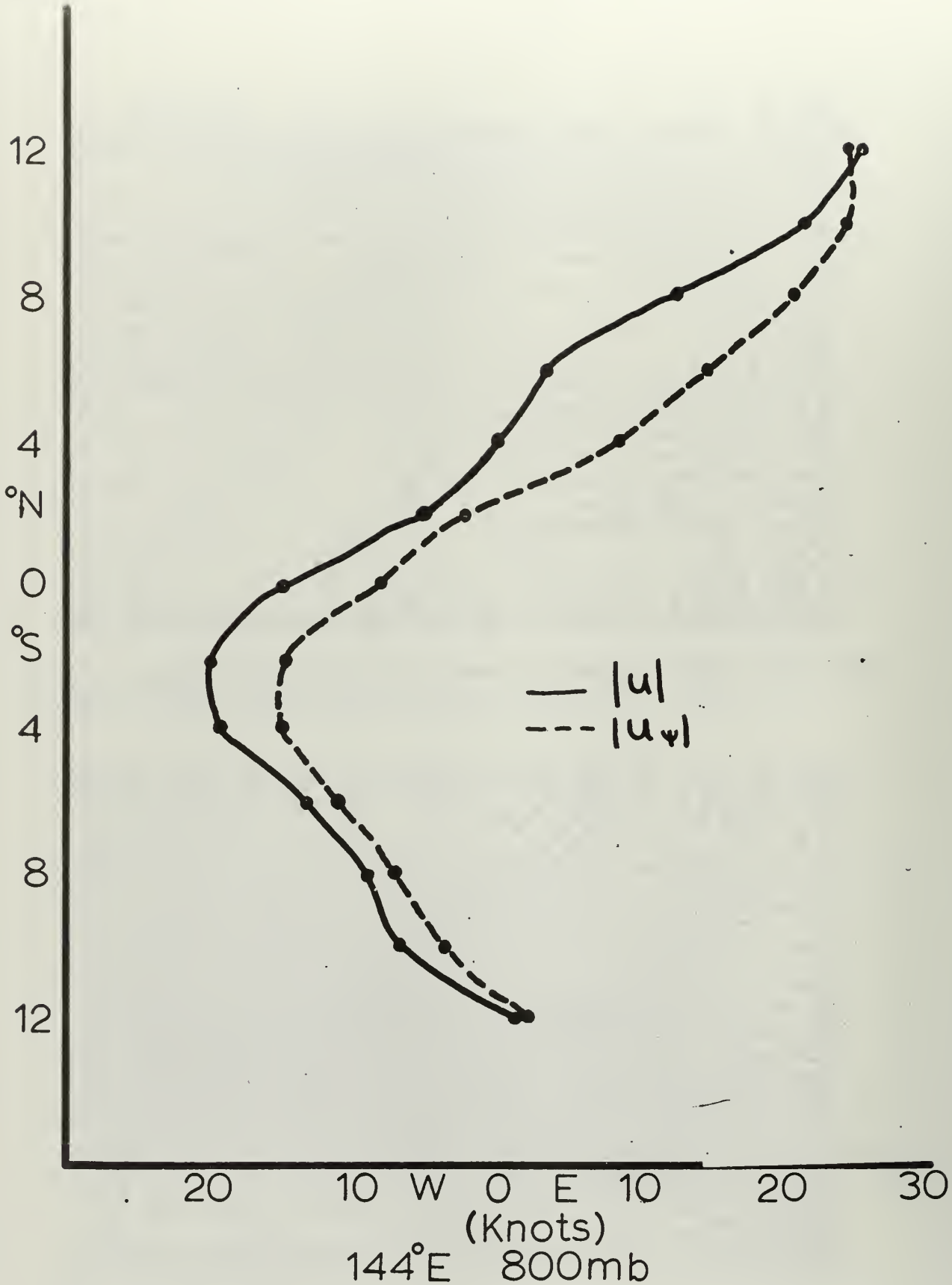

Fig. 18. A comparison of the input and non-divergent wind values.

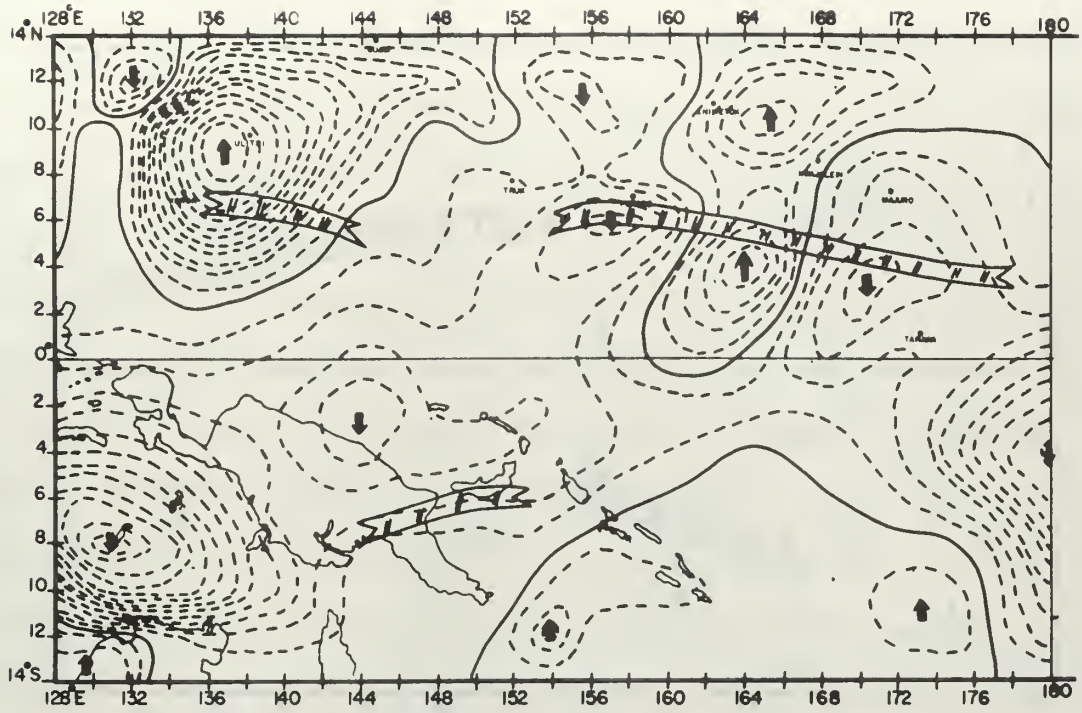

Fig. 19. Total vertical velocity at 900 mbs, 00Z 1 March 1965. Arrows indicate direction. Interval is 10×10^{-5} mbs sec^{-1}.

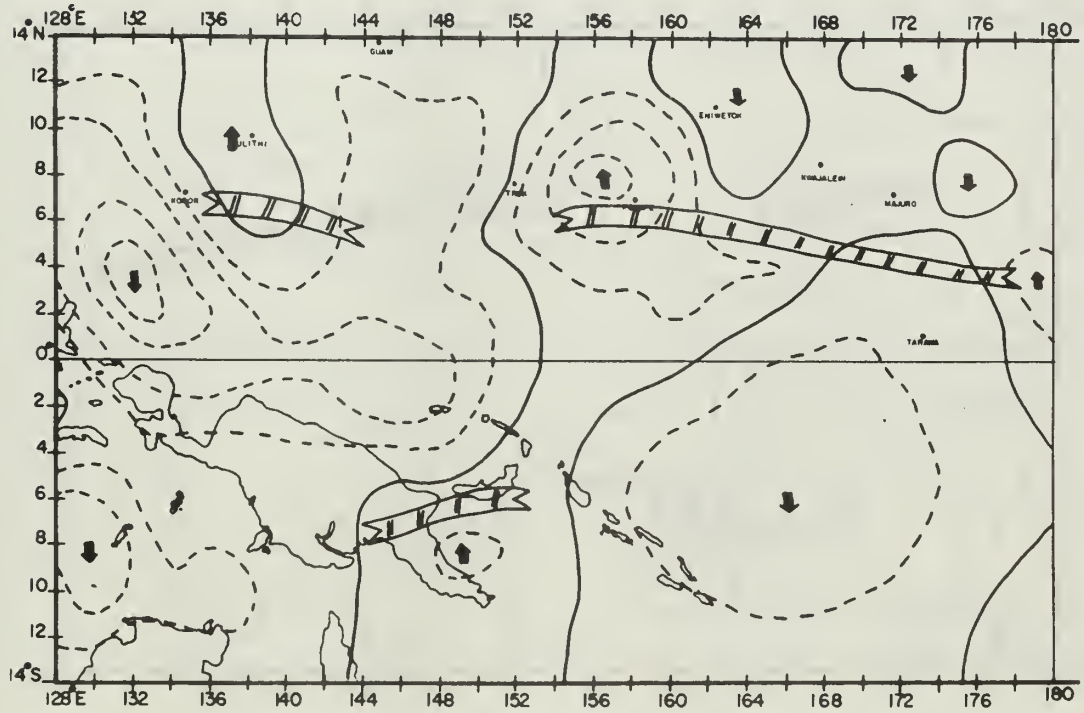

Fig. 20. Same as above except 700 mbs.

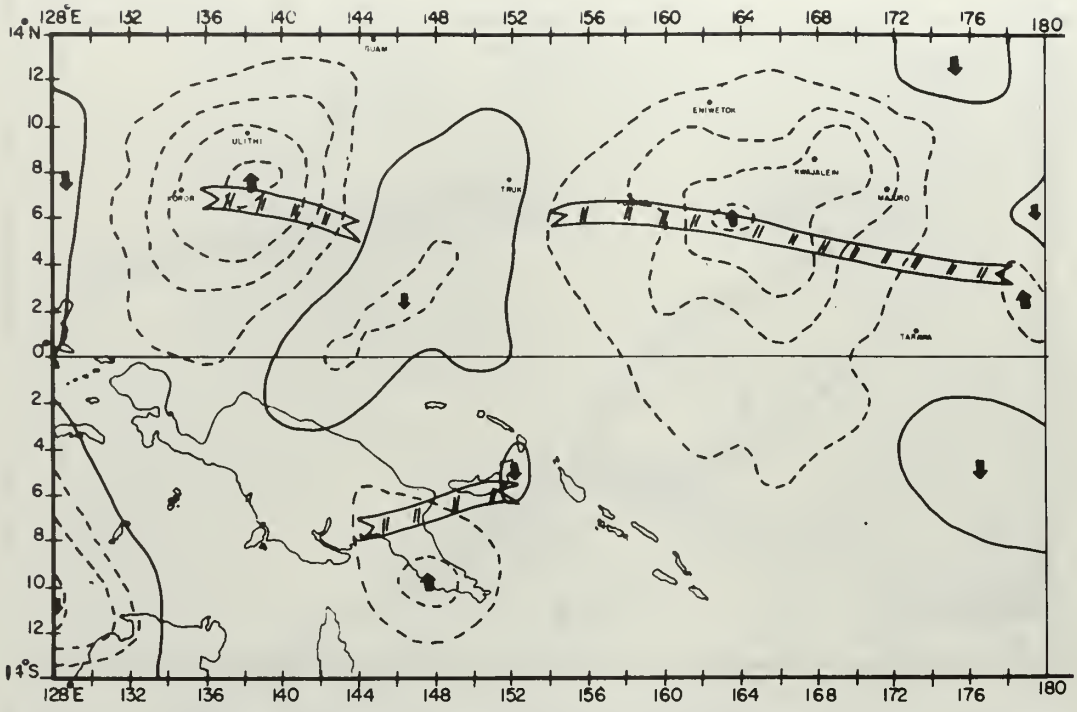

Fig. 21. Total vertical velocity at 500 mbs, 00Z 1 March 1965. Arrows indicate direction, interval is 10×10^{-5} mbs sec^{-1}.

Fig. 22. Same as above except 300 mbs.

Two points were chosen in the vicinity of the ITCZ, one at 164°E, 4°N in the eastern portion of the neph and a second at 138°E, 6°N in the western section, and a graph showing the variation of ω in the vertical was constructed (Fig.23). Typical magnitudes were found on the order of 50 to 80 x 10^{-5} mbs sec^{-1} (rising) in the frictional layer, decreasing to less than 20 x 10^{-5} mbs sec^{-1} above the frictional layer and with a secondary maximum in the mid and upper troposphere. This corresponds to Krishnamurti's theory that two maxima exist in the ω field in the vertical, the lower caused primarily by the influence of frictional convergence, which drops off at intermediate levels, and the second maximum in the mid and higher troposphere, where more closed circulations are found.

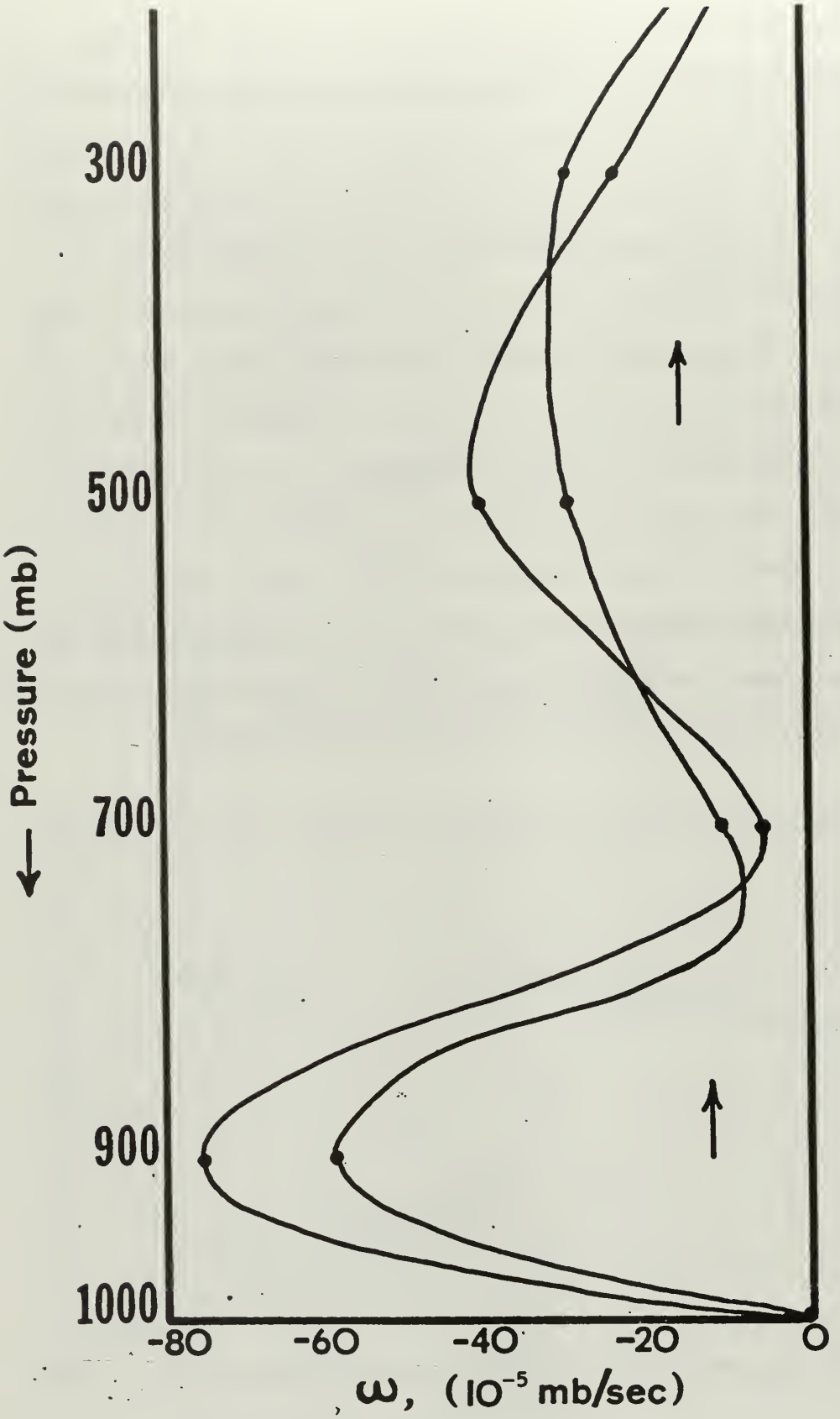

Fig. 23. Vertical variation of ω.

0000Z 3 March 1965

Synoptic situation. By the third of March we find that the nephanalysis for 0251Z (Fig. 24), from Tiros IX orbits 480-482, indicates that the Intertropical Convergence Zone is undergoing a major change with the northern section weakening and a second ITCZ intensifying to the south, so that there are actually two ITC's at 00Z on 3 March. The northernmost is defined mostly by the cloud picture and the use of the water vapor channel two data from Tiros VII indicates that it is most intense below about 20,000 feet.

The southern ITCZ is well defined by both clouds and convergence of the wind field with the channel two data indicating it extends to greater than 30,000 feet. Since the southern ITCZ is better defined by the wind field, much of the discussion of the streamlines will concern this area.

It is interesting to note that the nephanalyses for the 1st through the 4th of March show the continuous sequence of events of the change in the ITCZ. This phenomenon has been observed before by Airborne Early Warning Squadron 4 which made daily flights in the Eastern Pacific equatorial region for a period of 1½ months in 1957, during which time it was observed that the ITCZ intermittently moves rapidly north, dissipates, and reforms in the south (Roth, 1958).

The surface pressure analysis (Fig. 25) does not show the change in synoptic situation so dramatically, with the off season front still trailing down into the tropic region

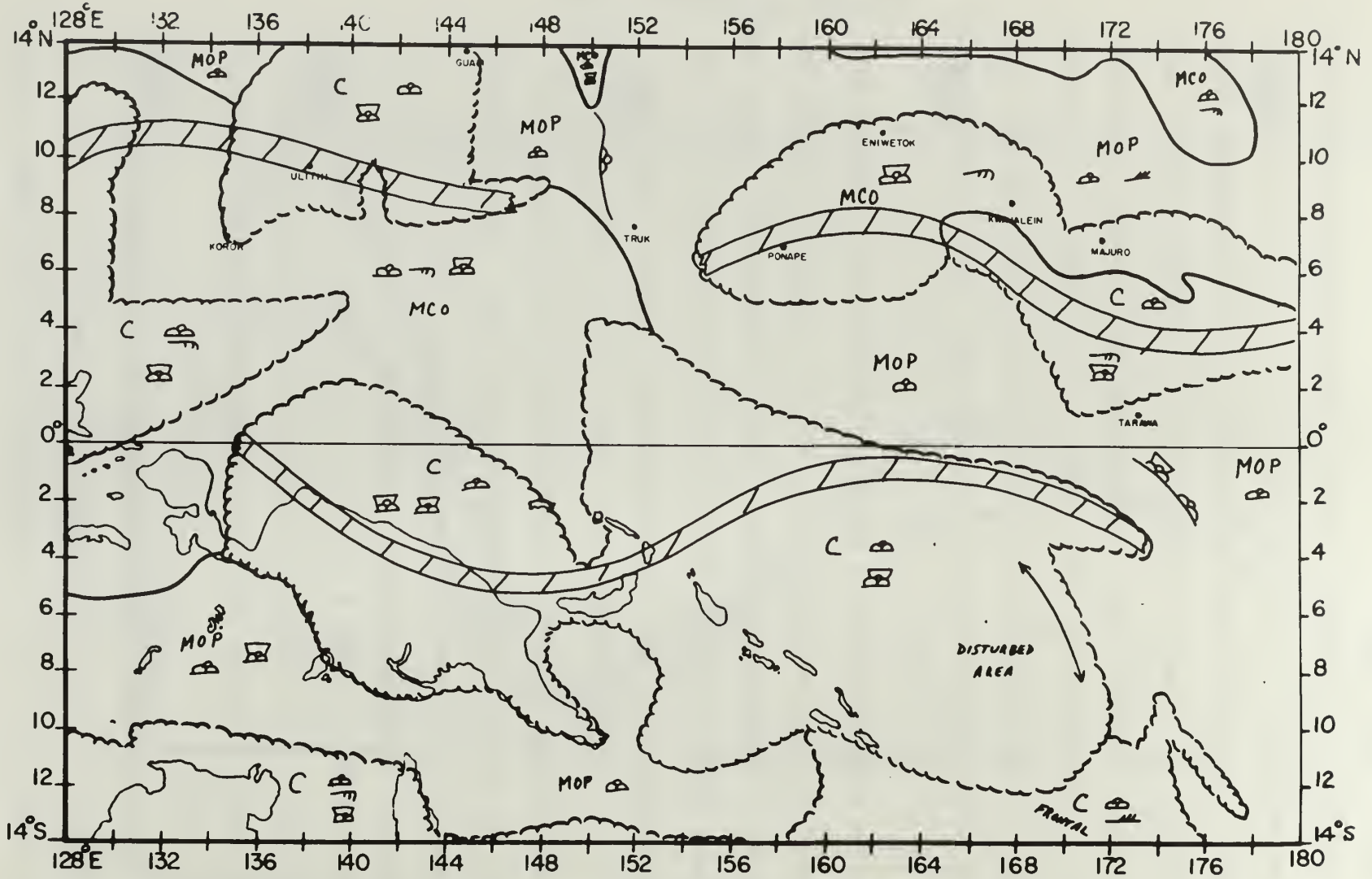

Fig. 24. Nephanalysis for 0251Z 3 March 1965. Standard symbols are used. ITCZ's are shown as cross-hatched lines.

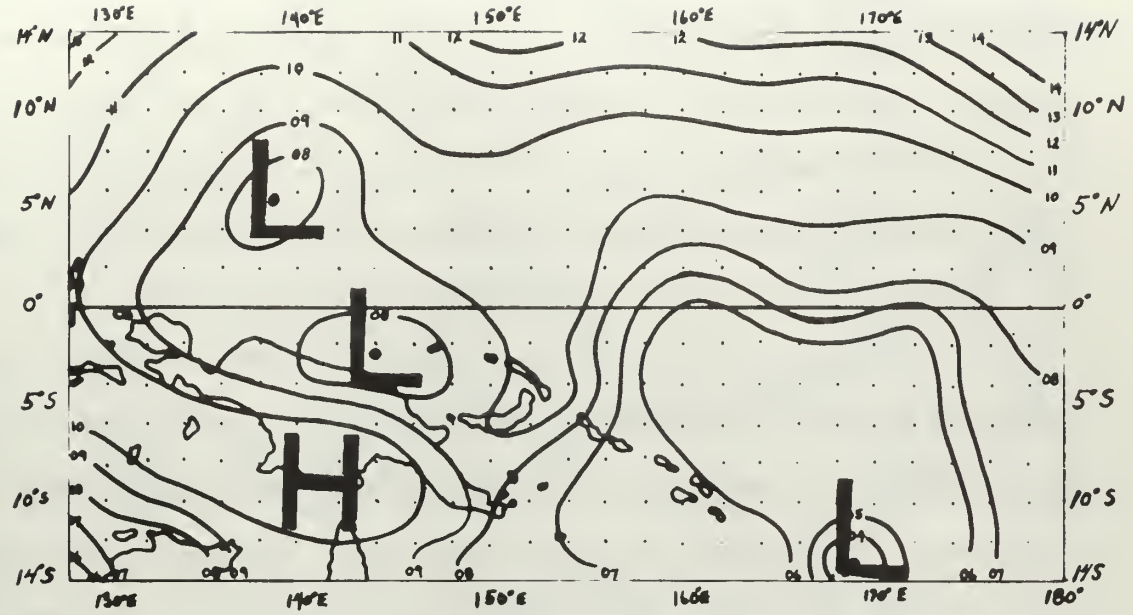

Fig. 25. Surface pressure field, 00Z 3 March 1965. Interval, 1 millibar.

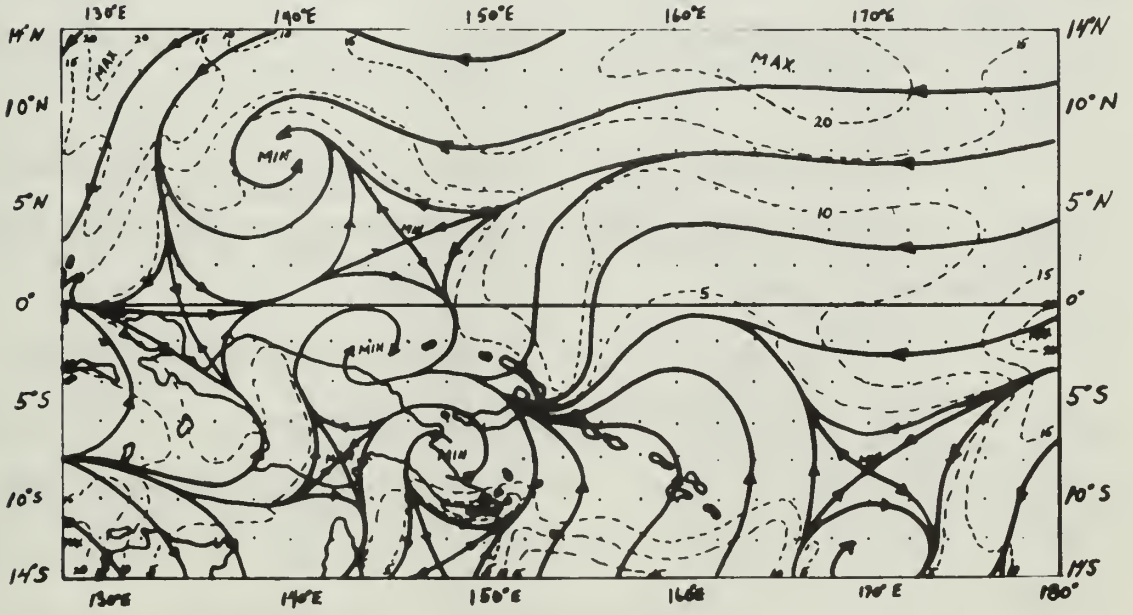

Fig. 26. Streamlines and isotachs at 1000 mbs, 00Z 3 March 1965. ——— streamlines, ----- isotachs. Isotach interval, 5 knots.

with low pressure extending northwest across the equator and a 1010 mb ridge located over the southern half of New Guinea. The streamlines and isotachs at the surface (Fig. 26) also support the pressure analysis, although we would expect a little more cross-isobar flow near the equator because of the diminished Coriolis parameter.

It is the authors' opinion that the anticyclonic and cyclonic eddies to the south and north of New Guinea, respectively, are caused by the effect of the mountainous terrain of New Guinea on the wind flow. The cyclonic circulation in the north hemisphere has weakened considerably since the 1st of March when it extended through several levels. On the 3rd it is only indicated by a slight wave at 850 mbs (Fig. 27) and disappears completely above that level. The southern ITCZ is well defined by the 850 mb streamlines and there is an excellent correlation with the nephanalysis.

The streamlines also indicate a reason for the weakening of the northern ITCZ, as divergence is indicated near the middle of the zone.

As we go upward in the atmosphere (Fig. 28), we can see that all trace of the cyclonic circulation to the north has disappeared but that the anticyclonic ridge over the south of New Guinea intensifies with height (Figs. 29, 30) and becomes a closed circulation by 300 mbs with outflow taking place.

We also find that we now have some divergence taking place over the southern ITCZ. The Subtropical Highs have

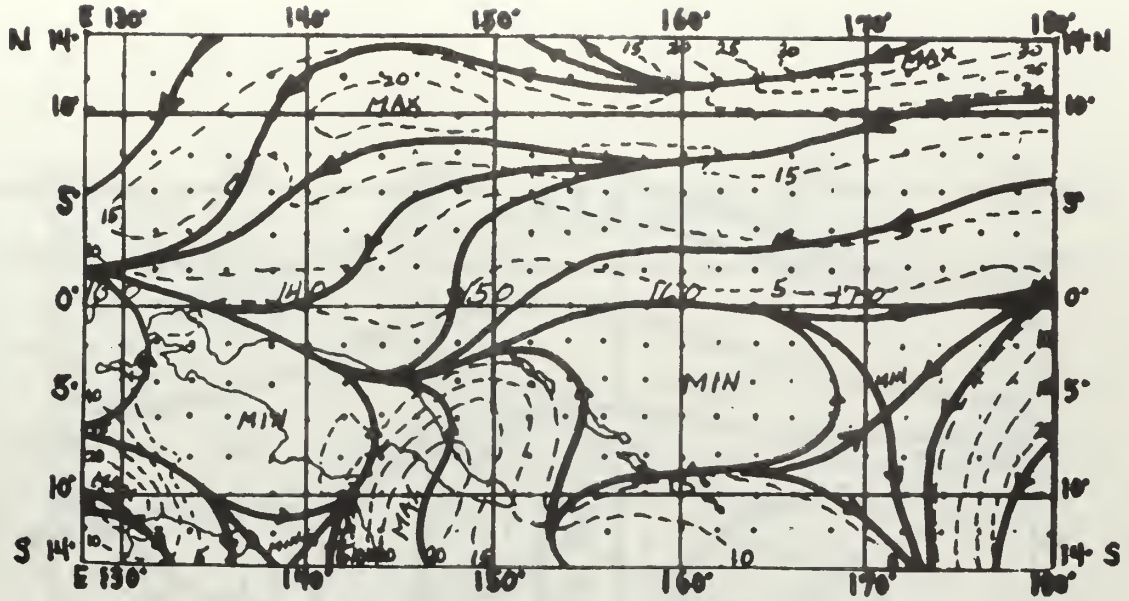

Fig. 27. Streamlines and isotachs at 850 mbs, 00Z 3 March 1965. ——— streamlines, ----- isotachs. Isotach interval, 5 knots.

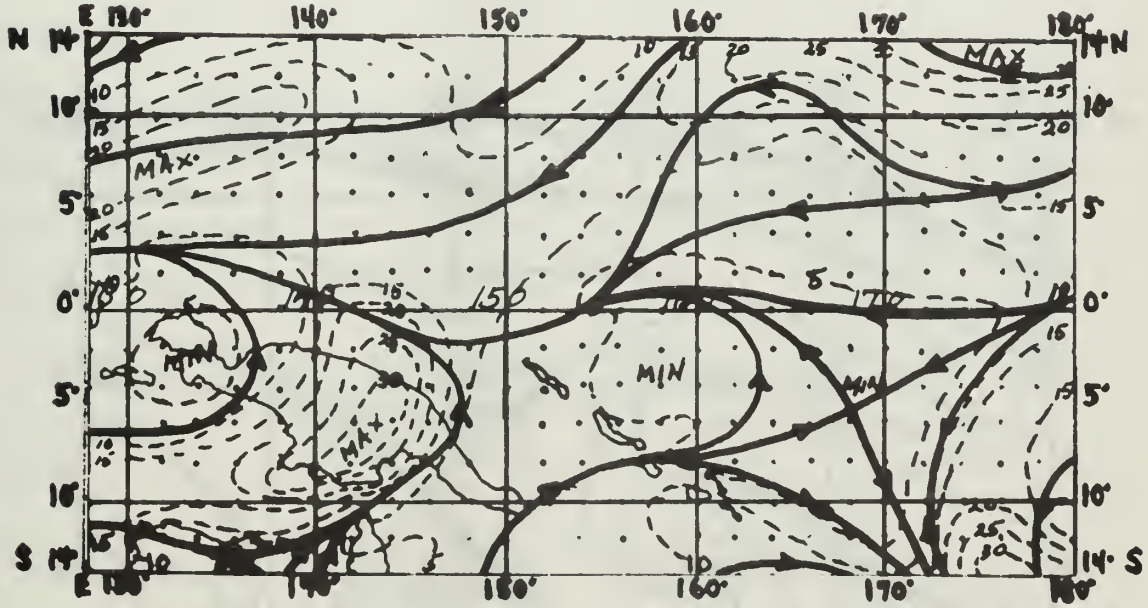

Fig. 28. Streamlines and isotachs at 700 mbs, 00Z 3 March 1965. ——— streamlines, ----- isotachs. Isotach interval, 5 knots.

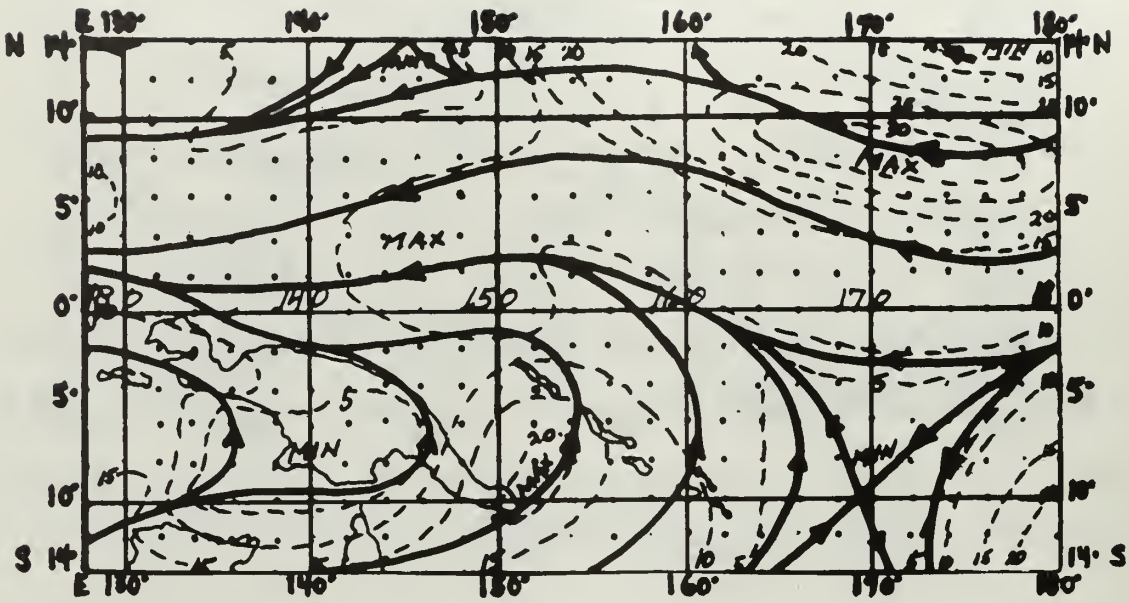

Fig. 29. Streamlines and isotachs at 500 mbs, 00Z 3 March 1965. ——— streamlines, ----- isotachs. Isotach interval, 5 knots.

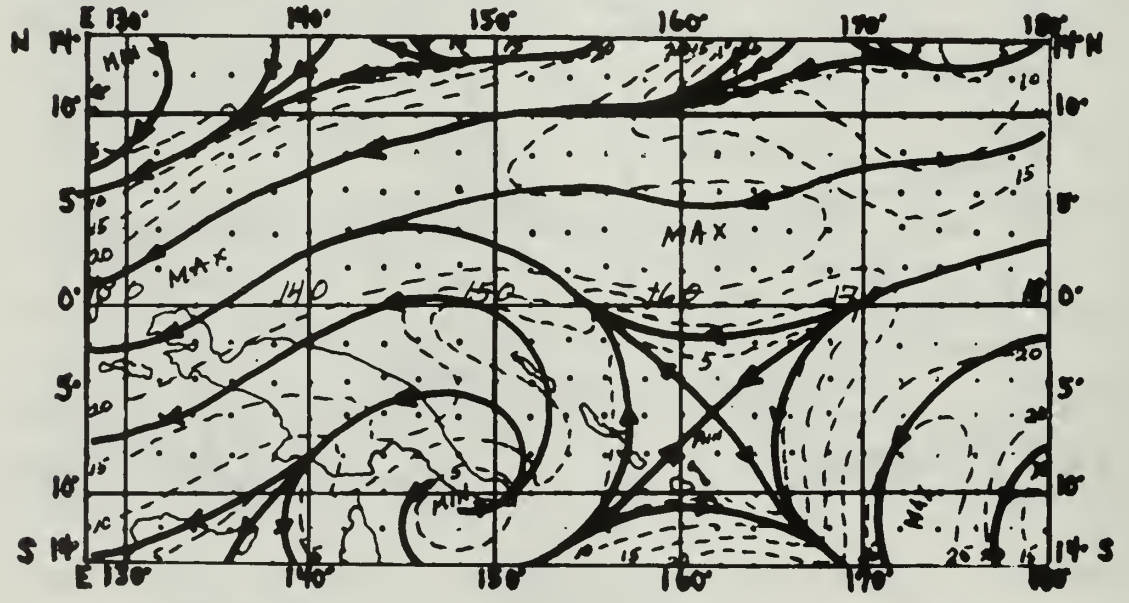

Fig. 30. Streamlines and isotachs at 300 mbs, 00Z 3 March 1965. ——— streamlines, ----- isotachs. Isotach interval, 5 knots.

moved equatorward and they can be seen clearly at 200 mbs (Fig. 31). The anticyclonic circulation persists at this level along with the divergence over the northern coast of New Guinea. There is now some convergence a little to the north of this area.

By looking at the temperature structure at low, intermediate and high levels (Figs. 32-34), we can see the anticyclonic ridge appears cold near the surface and the cyclonic circulation to the north is warm core. There is a persistent warm area to the southeast. What might be considered an anomaly is the fact that the region within 3 or 4 degrees latitude of the equator on both sides appears to be relatively cool at all levels compared to the surrounding area and this had a great effect on the calculated geopotential heights. When one notes that this is an area of considerable cloudiness and moisture with high evaporation, it is more explainable (Riehl, 1954). The temperature at the levels shown are the smoothed temperatures that were computed in the program and used in subsequent calculations.

Output. Geopotential heights were built up from the surface pressure and the vertical temperature structure by the use of the standard atmosphere for the 3rd of March (Figs. 35-39). Although the heights are not used in further calculations, they were done as a matter of interest to compare with Riehl's model (Fig. 13b) (Riehl and Malkus, 1958). The geopotential heights do not indicate the extreme height anomaly that Riehl found at high levels over

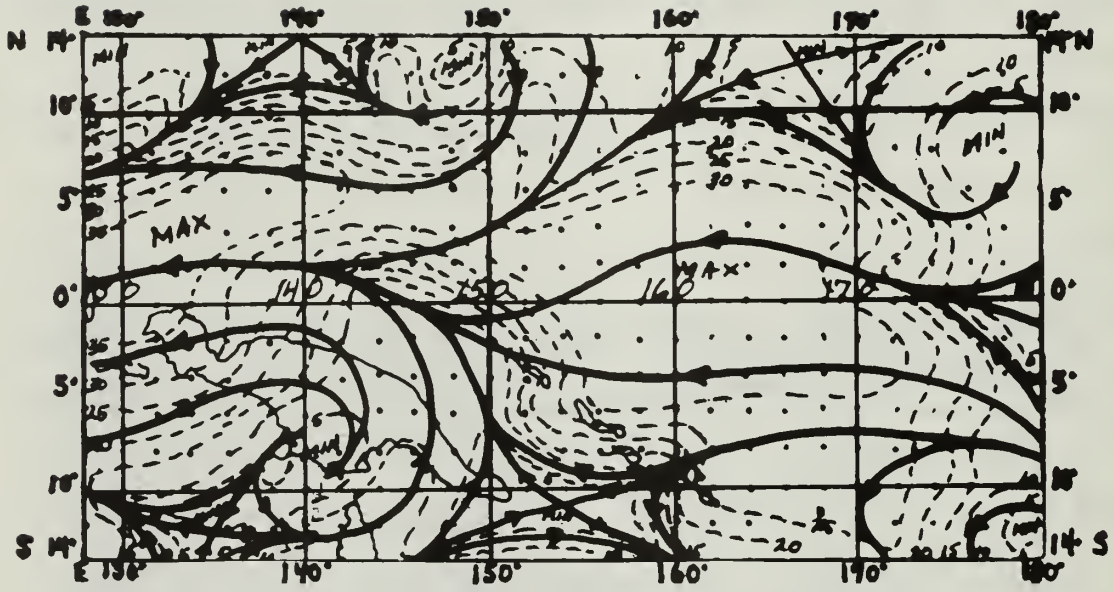

Fig. 31. Streamlines and isotachs at 200 mbs, 00Z 3 March 1965. ——— Streamlines, ----- isotachs. Isotach interval, 5 knots.

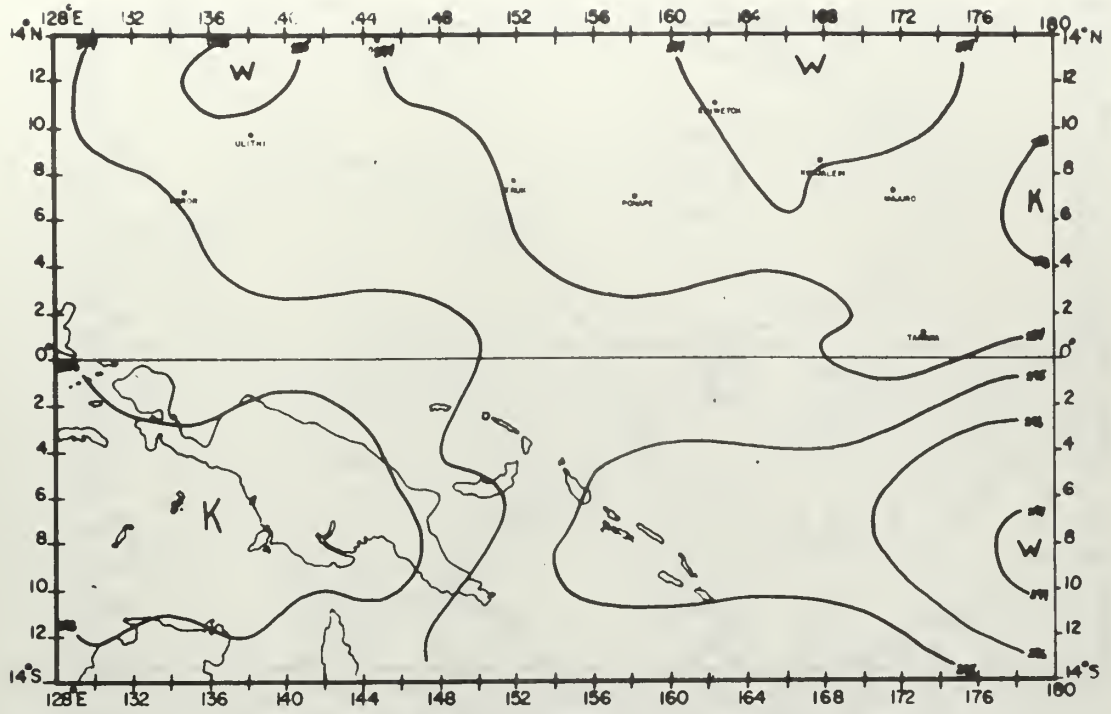

Fig. 32. Temperature at 900 mbs, 00Z 3 March 1965. Temp. in degrees Kelvin. Isotherm interval, 1 degree.

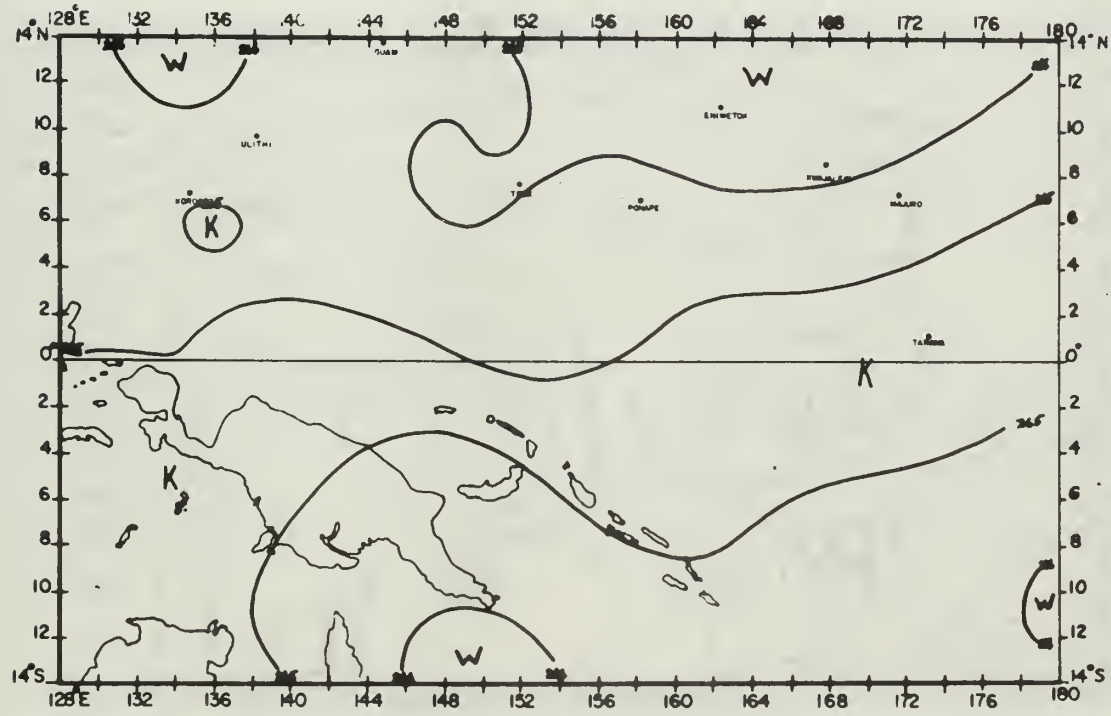

Fig. 33. Temperature at 500 mbs, 00Z 3 March 1965. Temp. in degrees Kelvin. Isotherm interval, 1 degree.

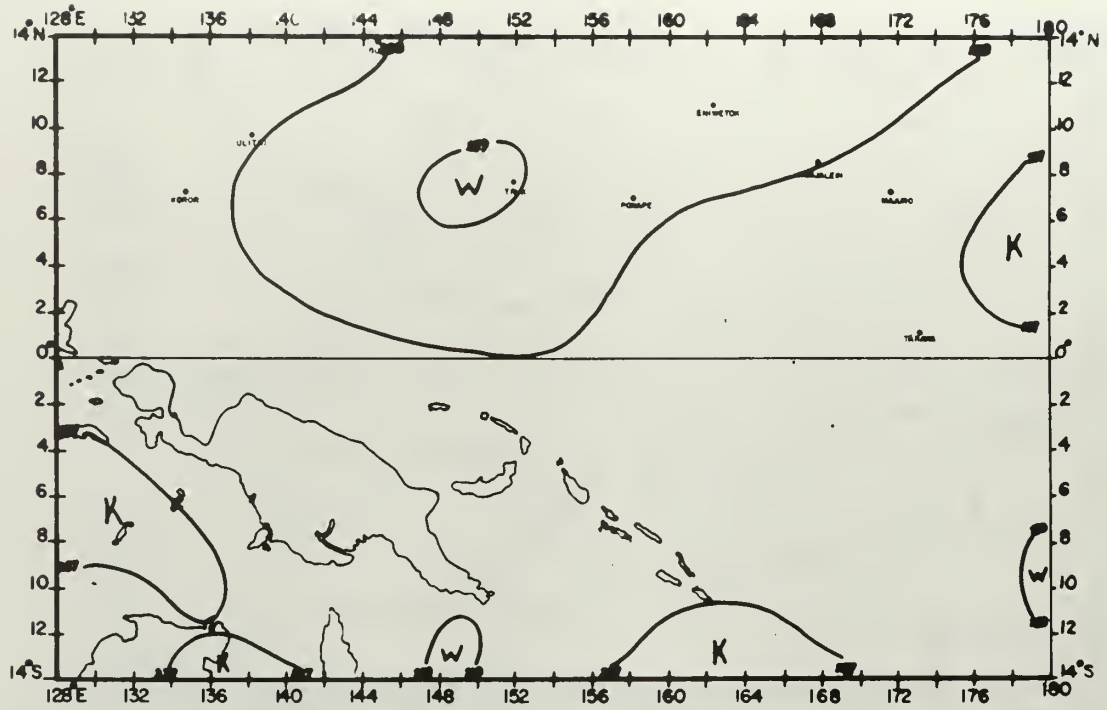

Fig. 34. Temperature at 300 mbs, 00Z 3 March 1965. Temp. in degrees Kelvin. Isotherm interval, 1 degree.

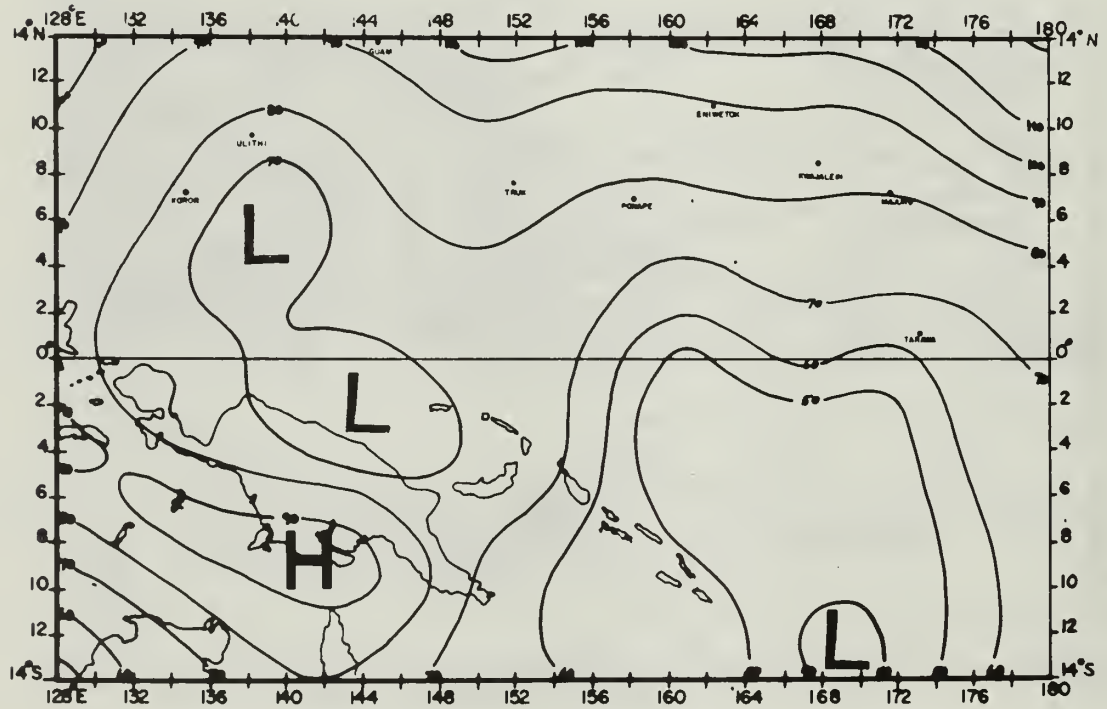

Fig. 35. Geopotential height at 1000 mbs, 00Z 3 March 1965. Heights in meters. Interval, 10 meters.

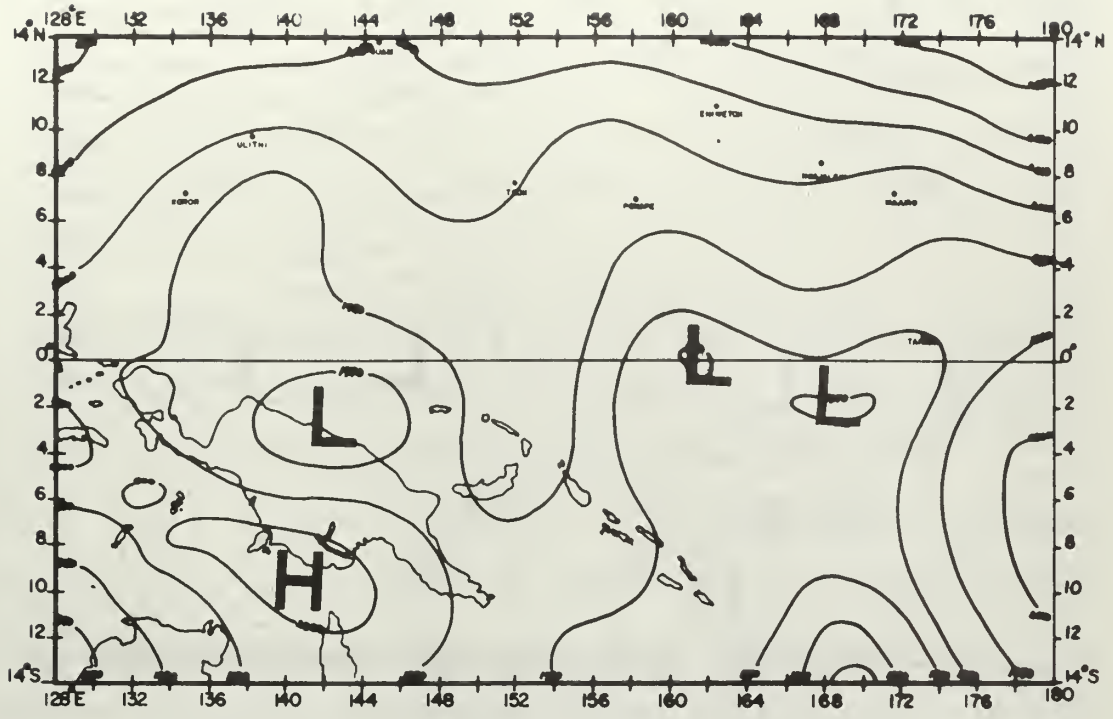

Fig. 36. Geopotential height at 800 mbs, 00Z 3 March 1965. Heights in meters. Interval, 10 meters.

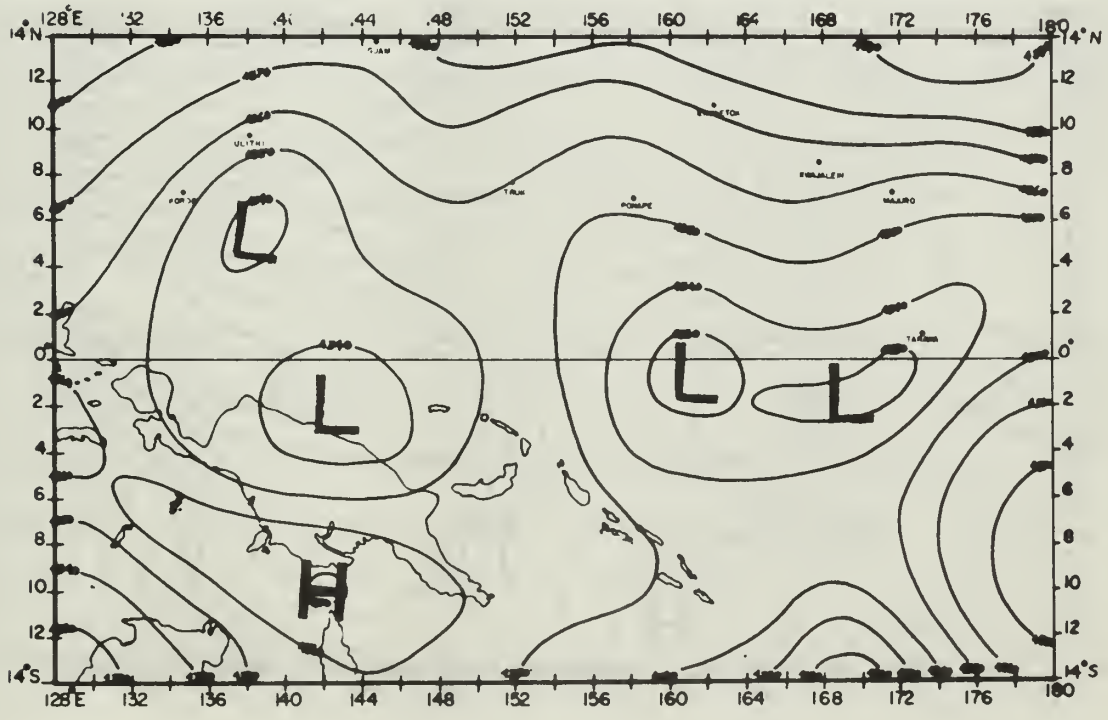

Fig. 37. Geopotential height at 600 mbs, 00Z 3 March 1965. Heights in meters. Interval, 10 meters.

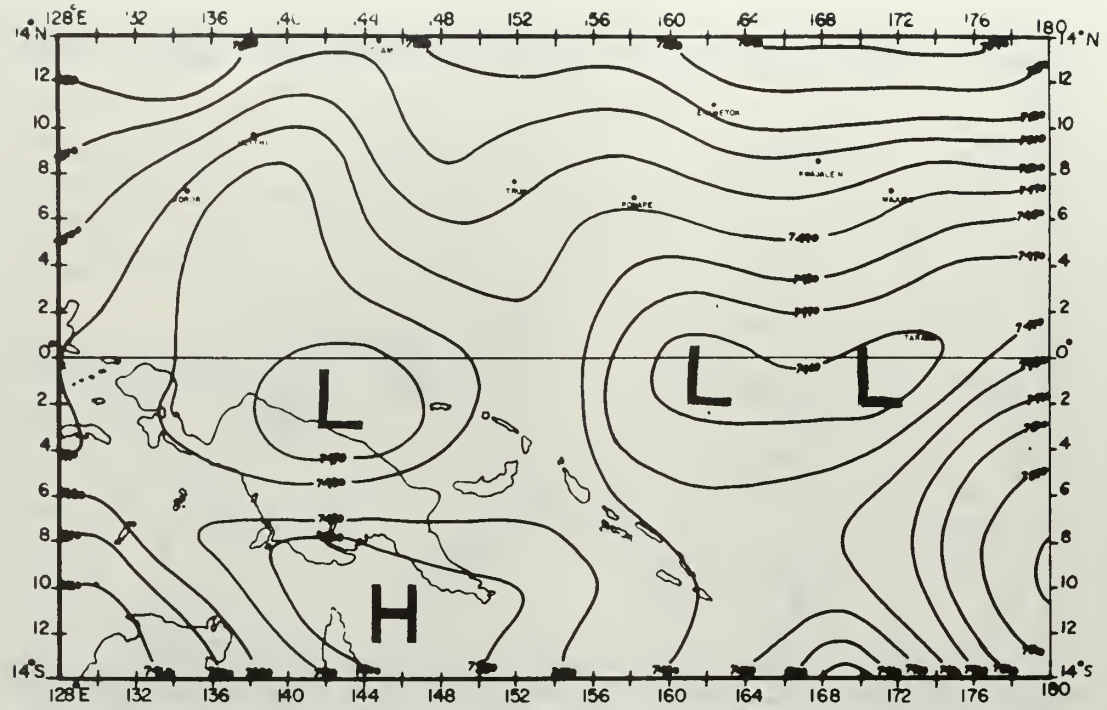

Fig. 38. Geopotential height at 400 mbs, 00Z 3 March 1965. Heights in meters. Interval, 10 meters.

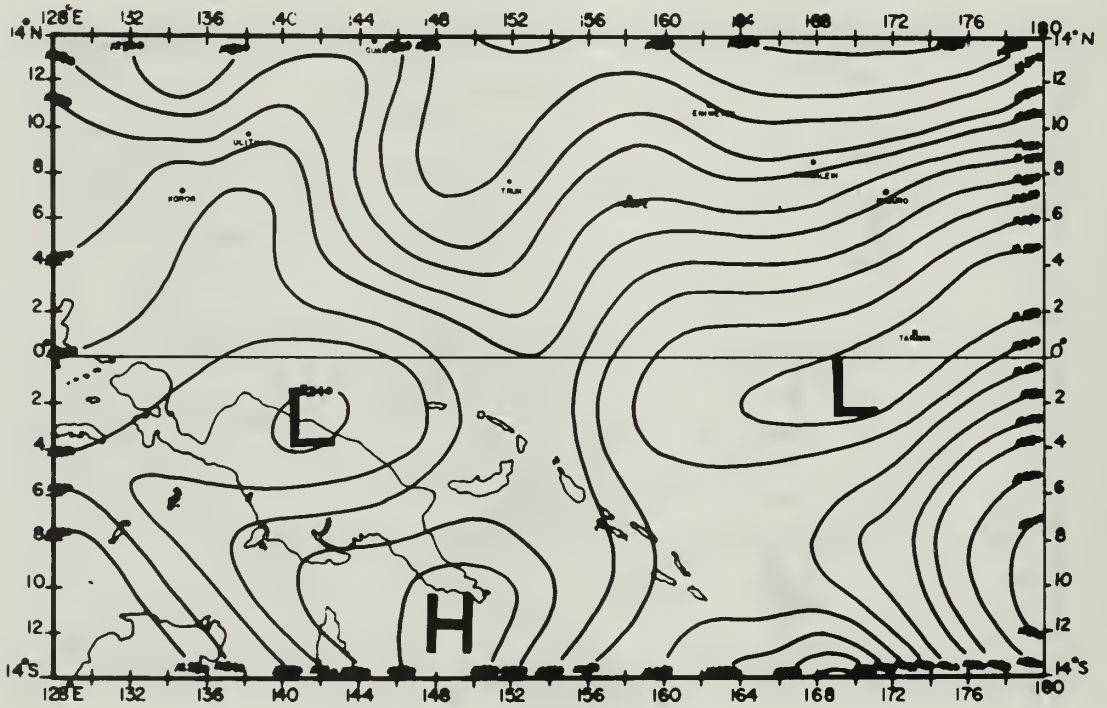

Fig. 39. Geopotential height at 200 mbs, 00Z 3 March 1965. Heights in meters. Interval, 10 meters.

the ITCZ, instead low pressure was found. This is believed to be caused by the difference in the vertical temperature of Riehl's model (Fig. 13a) as compared to observed temperatures on 3 March. The warm anomalies up to 200 mbs were not found.

A comparison of the 200 mb streamlines (Fig. 31) with the geopotential height at 200 mbs (Fig. 39) shows little resemblance to one another, which might be an indication that an observed height analysis, if enough data were available, would be considerably different from the geopotential height. This is a further point to be taken into account when deciding whether to compute the non-divergent stream function from the geopotential height or alternately from the observed winds, as has been done here.

Static stability. The dry static stability output at all levels indicates two main features, which are illustrated by the values at 900 and 300 mbs (Figs. 40, 41). One is that values are slightly positive everywhere within the region on the 3rd of March. The second feature indicates what we might expect in the tropics, that the gradient of dry static stability is very small. The same situation had been found on 1 March. The cloud situation indicates that the moist static stability would be a significant factor and that much of the area would be conditionally unstable, leading to large contributions to the upward vertical velocities from the latent heat forcing function. This would be mostly true in the areas of extensive cumulus cloud coverage, such as the ITCZ.

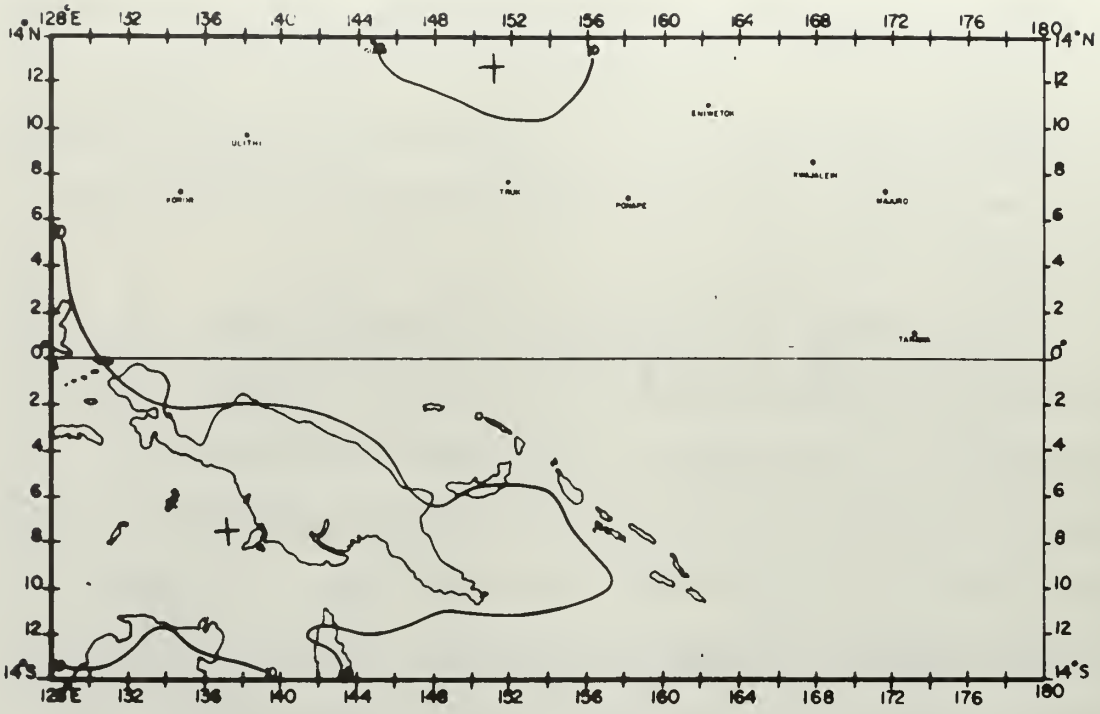

Fig. 40. Static stability at 1000 mbs, 00Z 3 March 1965. Interval, 10×10^{-3} meters^2 mbs^{-2} sec^{-2}.

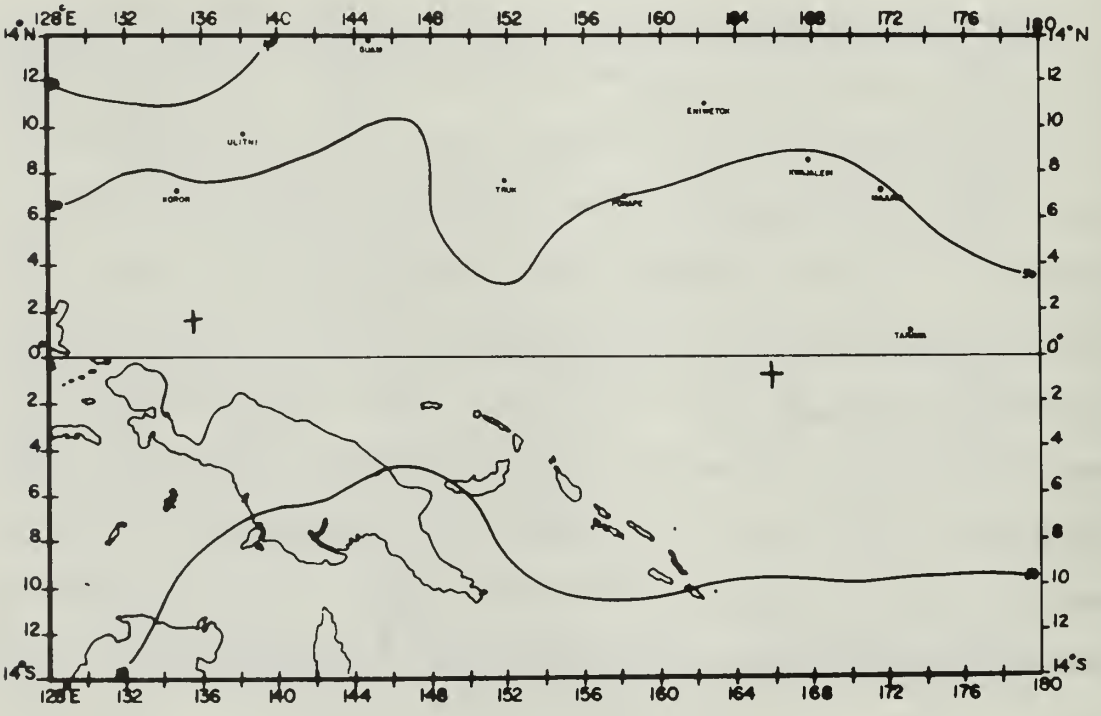

Fig. 41. Static stability at 300 mbs, 00Z 3 March 1965. Interval, 10×10^{-3} meters^2 mbs^{-2} sec^{-2}.

Vorticity. An example of the absolute vorticity output using the actual winds is shown at 1000 mbs (Fig. 42). It must be remembered that the signs of cyclonic and anticyclonic vorticity are reversed in the Southern Hemisphere so that negative values indicate cyclonic vorticity south of the equator. This introduces some confusion, especially in areas such as the closed - 10 x 10^{-6}/sec center at 178°E which is situated on the equator. The fact that the center extends into both hemispheres indicates anticyclonic vorticity in the northern part of the center and cyclonic in the southern half. This is not a contradiction if we take a look at the 1000 mb streamline chart (Fig. 26). The streamlines indicate a clockwise curvature and has a maximum in the isotachs south of the easterly winds in that area. Both of these facts lead to just the picture that is illustrated by the vorticity center. Anticyclonic vorticity to the north of the equator and cyclonic vorticity to the south.

The program takes the change of sign into account when computing vertical velocities from vorticity effects so that the sign of ω will be correct in both hemispheres.

Stream function. Computed non-divergent stream functions are shown at 1000, 800, 600, 400 and 200 mbs (Figs. 43-47) and a comparison with the streamlines at similar levels (Figs. 26-31) shows a striking similarity. A north-south cross-section was selected at random to see the actual correlation on the 3rd as compared to that found on the 1st.

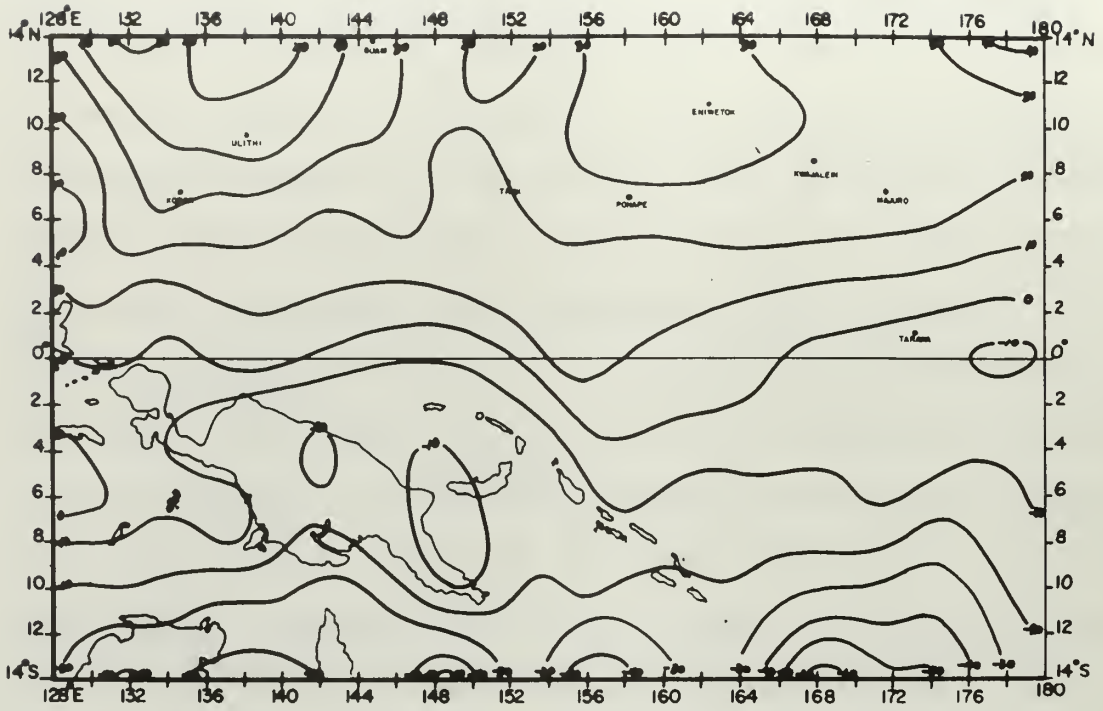

Fig. 42. Absolute vorticity at 1000 mbs, 00Z 3 March 1965. Interval, 10x 10^{-6} sec^{-1}.

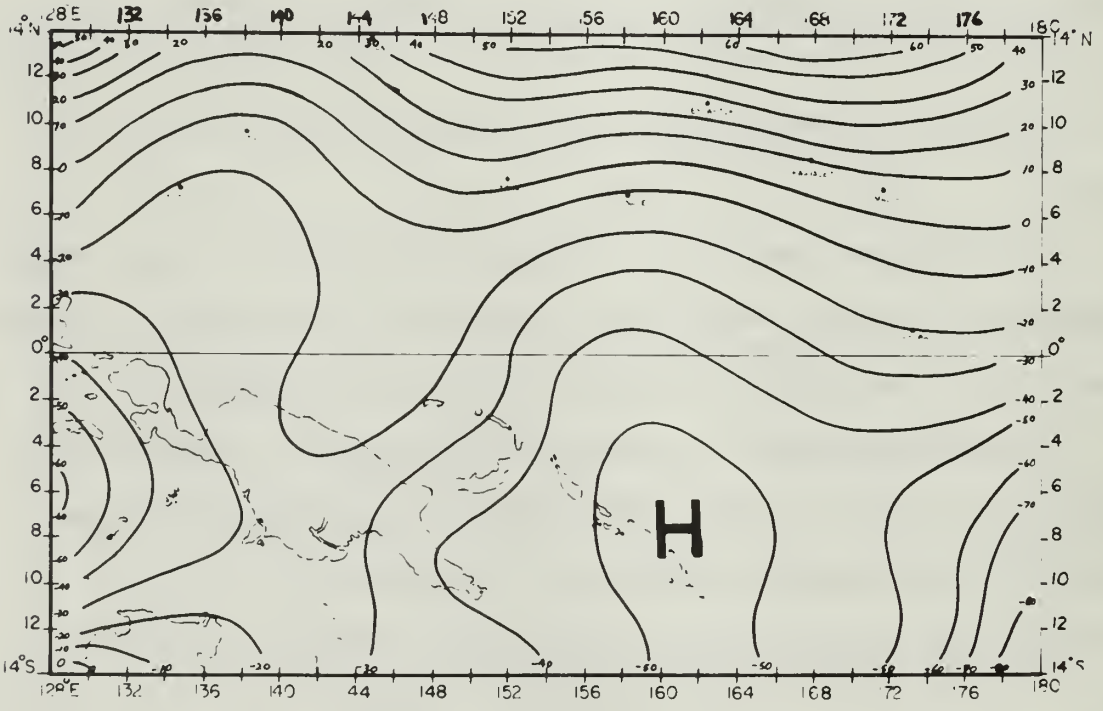

Fig. 43. Non-divergent stream function at 1000 mbs, 00Z 3 March 1965. Interval, 10x10^{-5} $meters^2$ sec^{-1}.

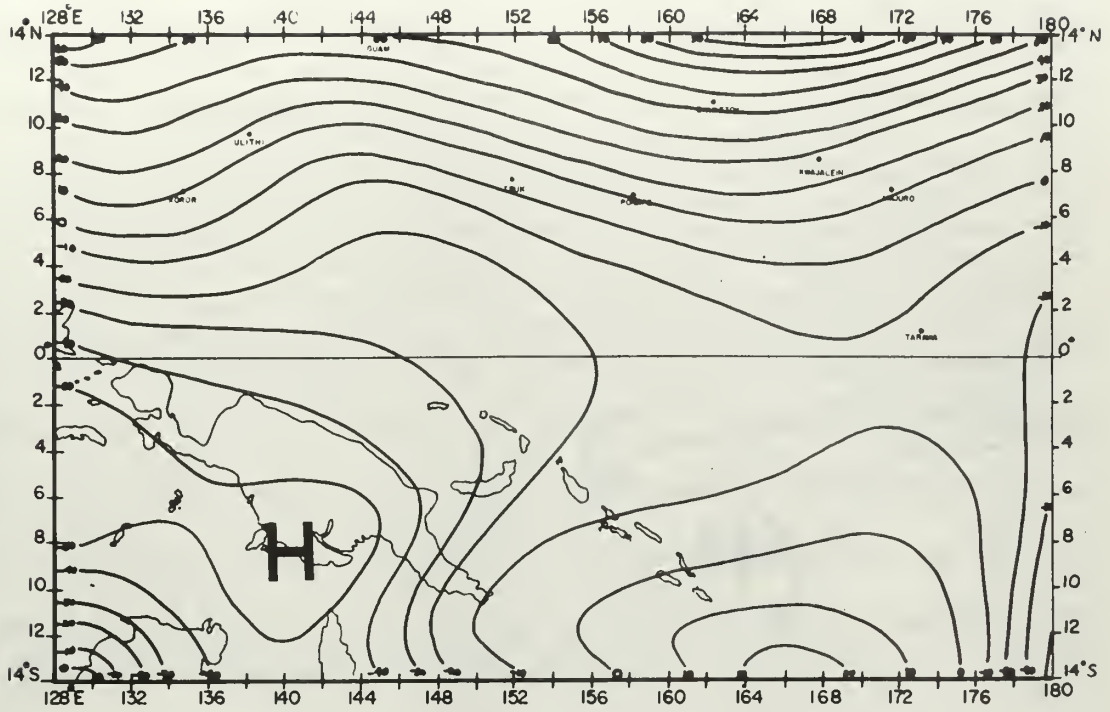

Fig. 44. Non-divergent stream function at 800 mbs, 00Z 3 March 1965. Interval, 10×10^{-5} meters^2 sec^{-1}.

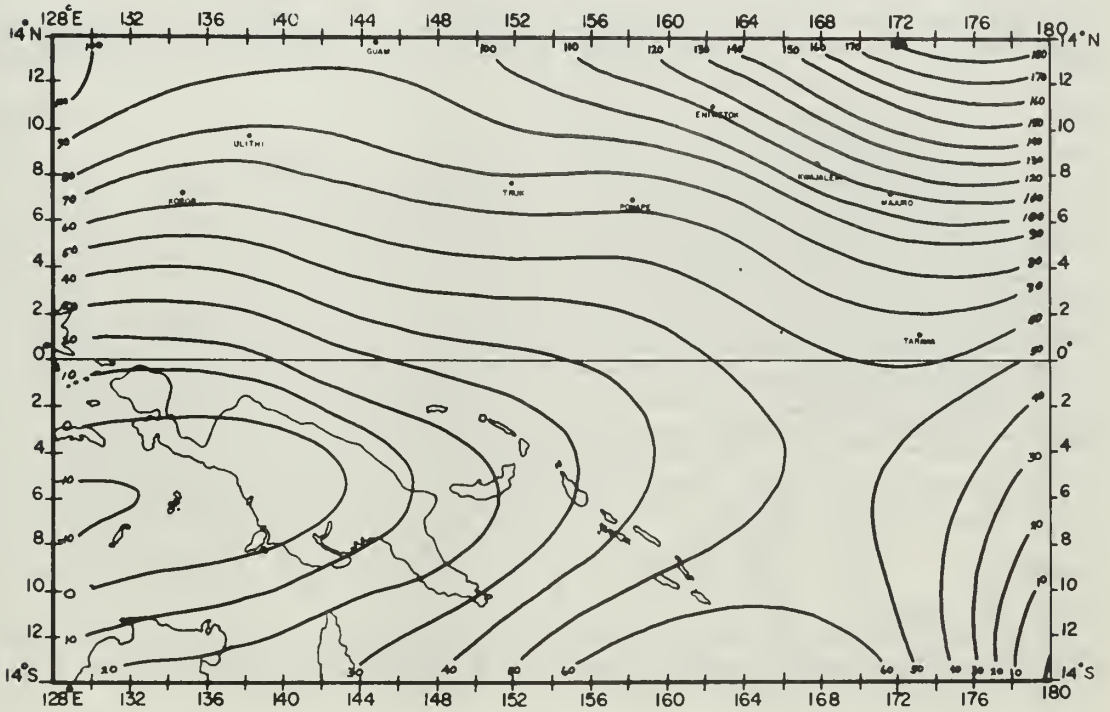

Fig. 45. Non-divergent stream function at 600 mbs, 00Z 3 March 1965. Interval, 10×10^{-5} meters^2 sec^{-1}.

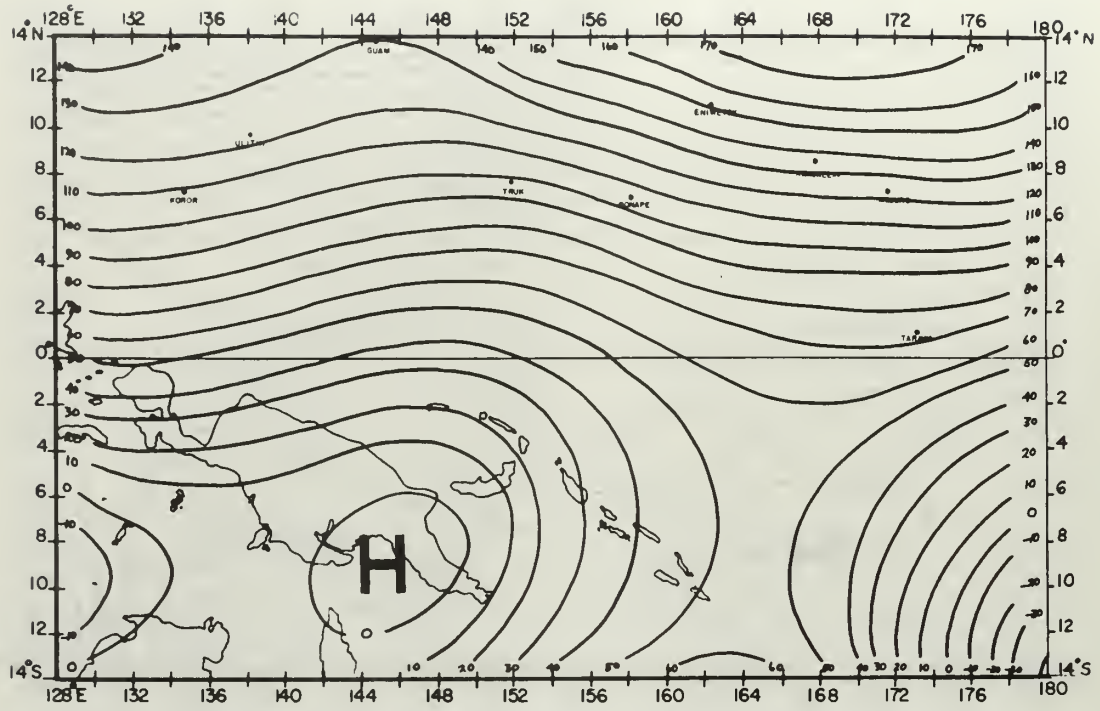

Fig. 46. Non-divergent stream function at 400 mbs, 00Z 3 March 1965. Interval, 10×10^{-5} meters^2 sec^{-1}.

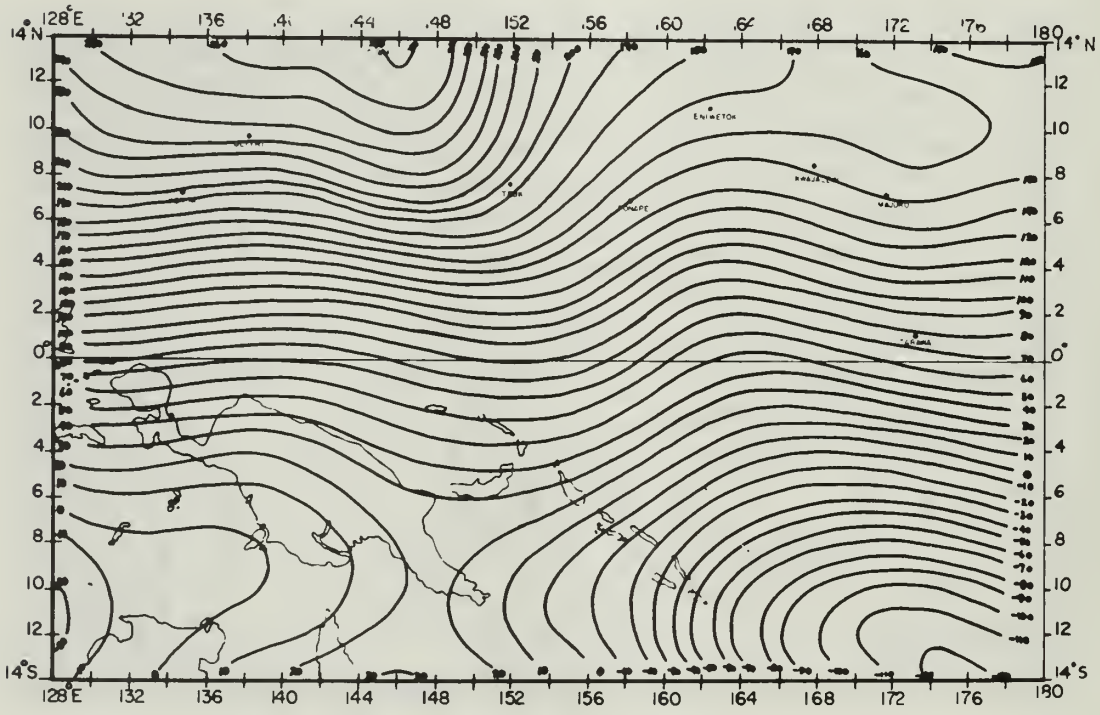

Fig. 47. Non-divergent stream function at 200 mbs, 00Z 3 March 1965. Interval, 10×10^{-5} meters^2 sec^{-1}.

The cross-section was taken at 140°E at 200 mbs. The actual winds were almost strictly zonal in this area so the entire wind was taken and compared to the zonal non-divergent component calculated from $u_\psi = -\frac{\partial \psi}{\partial y}$. The results (Fig. 48) show a remarkably close correlation, with some apparent opposing winds from the divergent component between 3°N and 3°S and between 5° and 9°S. Note that the true winds pass through a calm area about 8°S (Fig. 31) and change direction by almost 180° and the non-divergent component shows the same results. Near the centers of highs and lows we would expect a larger contribution from the divergent part of the wind.

Vertical velocity. The total vertical velocity in units of 10^{-5}mb/sec is shown at the output levels of 900, 700, 500 and 300 mbs (Figs. 49-52) with the ITCZ's superimposed as hatched double lines to observe the correlation, if any.

It must be remembered that the vertical velocities shown here do not include sensible heat, which should give a minor contribution in the tropics, and latent heat, which has been shown to be a major contributor to the upward vertical velocities in the tropics. We find a fairly good correlation with the cloud cover and the ITCZ's at 900 mbs (Fig. 49), with vertical velocities greater than 1 cm/sec upward and over 1.5 cm/sec downward. Rising vertical motions are found over 95 percent of the analyzed ITCZ's with two intense centers in the north and a weaker one to the

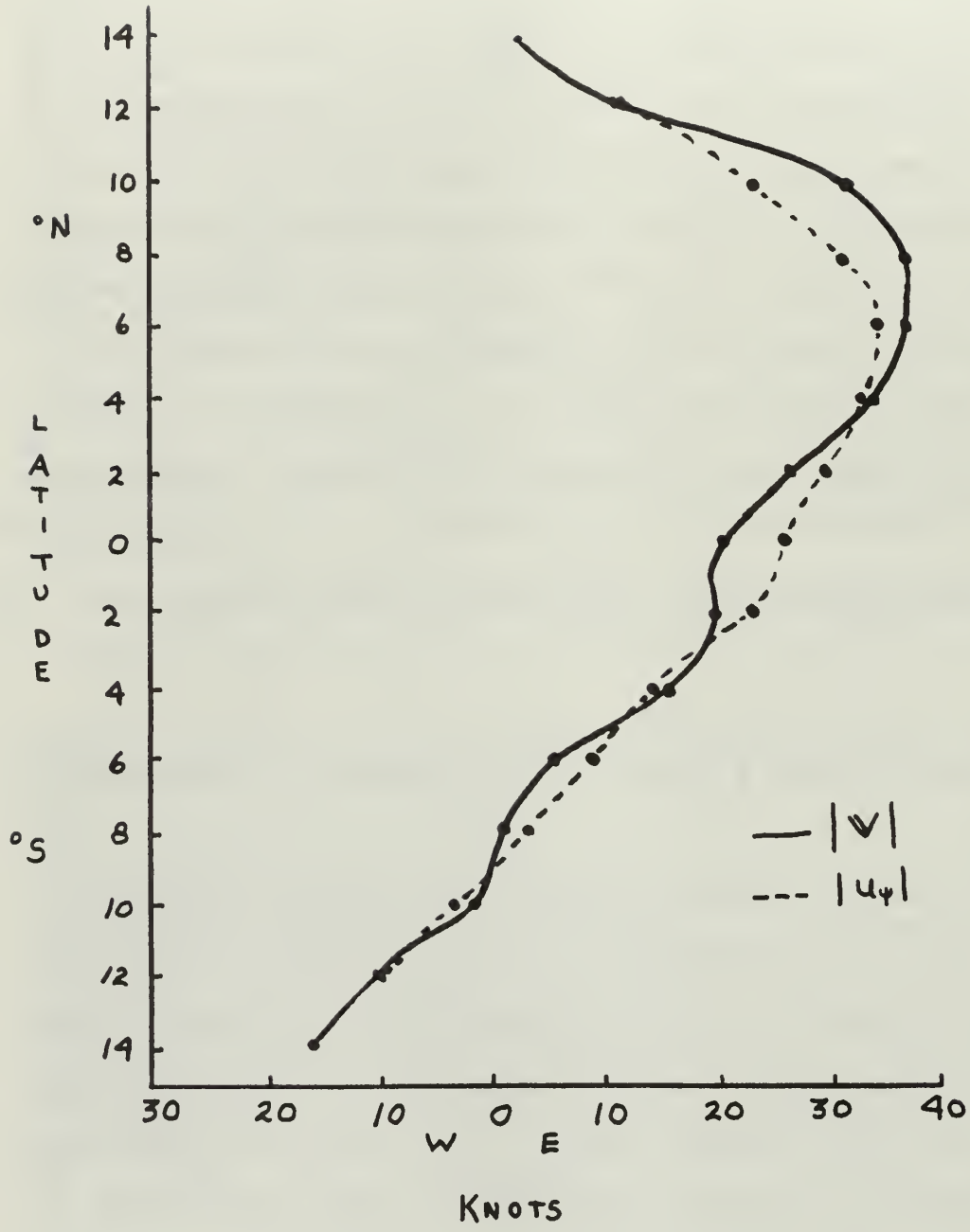

Fig. 48. North-South cross-section of actual wind speed versus zonal component of the non-divergent wind at 140° E, 200 mbs, 00Z 3 Mar. 1965.

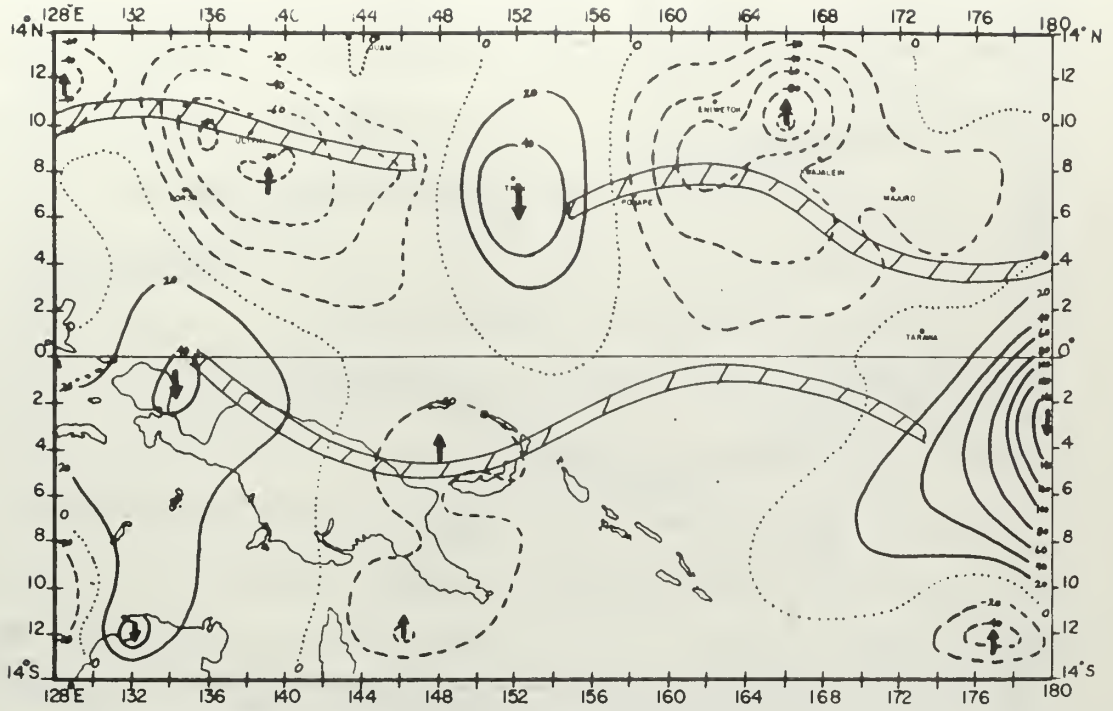

Fig. 49. Total vertical velocity at 900 mbs, 00Z 3 March 1965. ——— sinking, ····· neutral, ----- rising. ITCZ is cross-hatched. Interval, 20×10^{-5} mbs sec^{-1}.

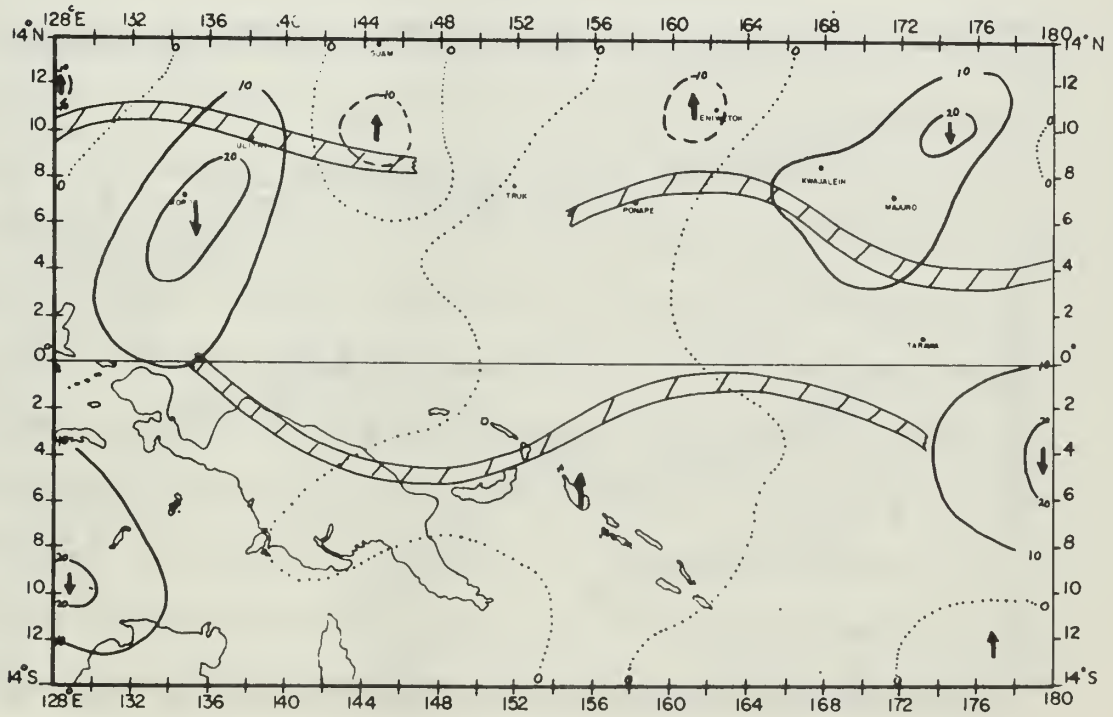

Fig. 50. Total vertical velocity at 700 mbs, 00Z 3 March 1965. ——— sinking, ····· neutral, ---- rising. ITCZ is cross-hatched. Interval, 10×10^{-5} mbs sec^{-1}.

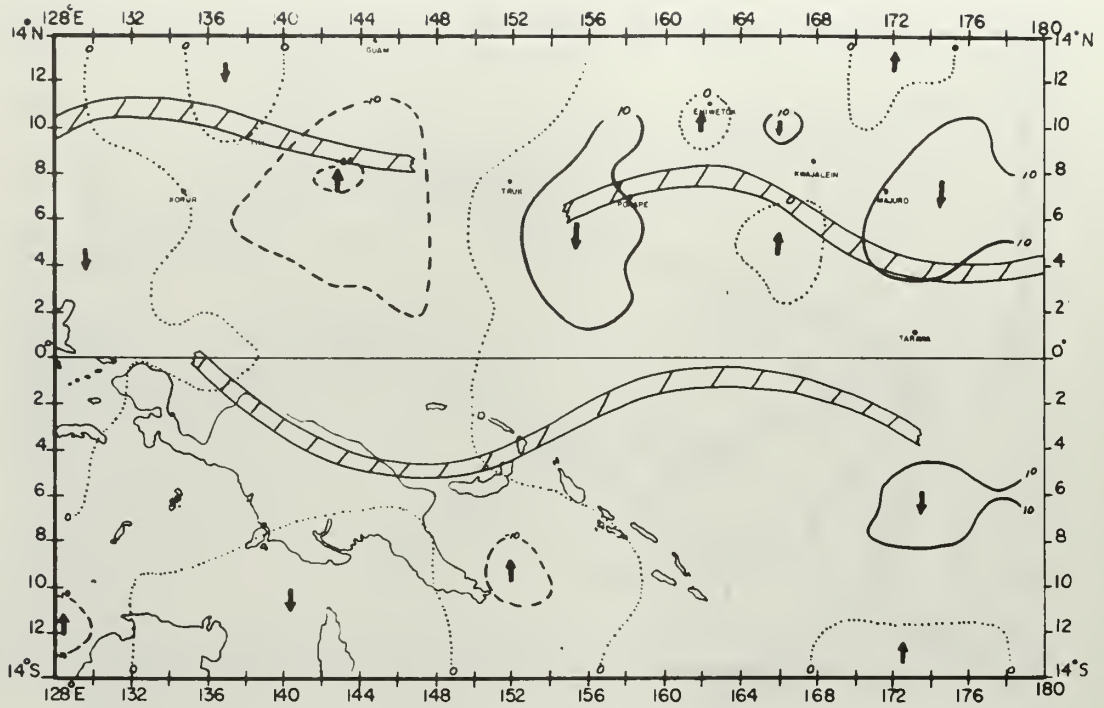

Fig. 51. Total vertical velocity at 500 mbs, 00Z 3 March 1965. ——— sinking, ····· neutral, --5-- rising. ITCZ is cross-hatched. Interval, $10x10^{-5}$ mbs sec^{-1}.

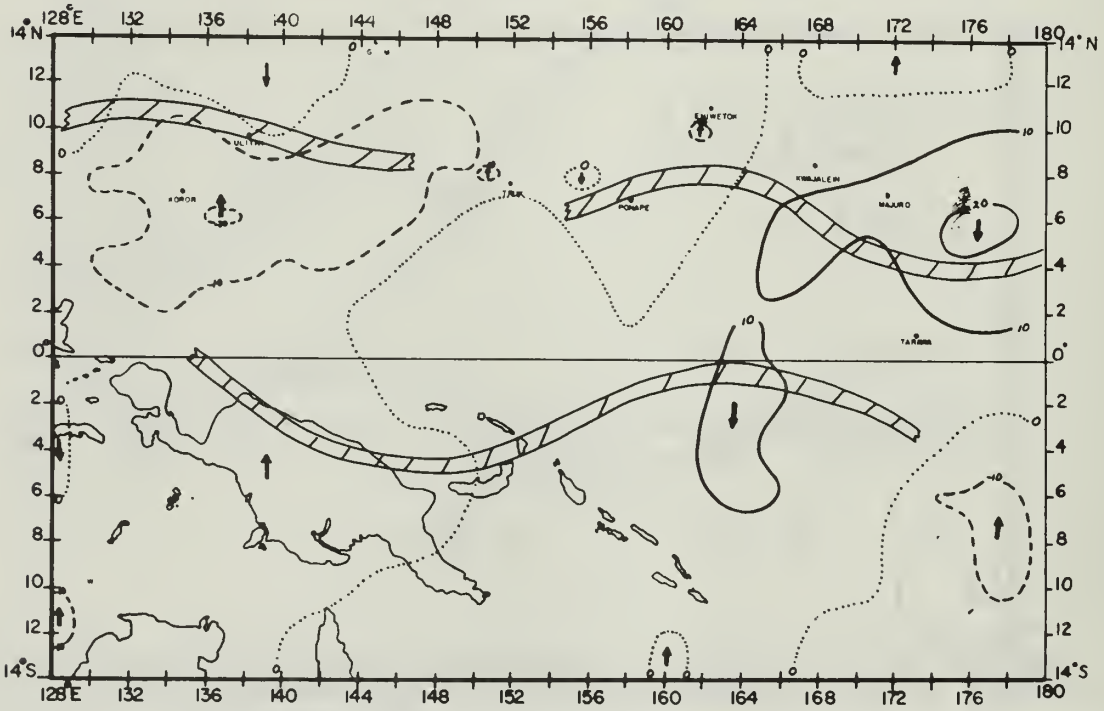

Fig. 52. Total vertical velocity at 300 mbs, 00Z 3 March 1965. ——— sinking, ····· neutral, ----- rising. ITCZ is cross-hatched. Interval, $10x10^{-5}$ mbs sec^{-1}.

south, indicating that the northern ITCZ may be more active near the surface. The higher levels show a much poorer correlation with the ITCZ's. The 700 mb output (Fig. 50) does show rising motions over most of the southern ITCZ and part of the northern one. Maximum vertical velocities are of the order of .25 cm/sec. The correlation at 500 mbs (Fig. 51) is even worse except in one portion of the northern ITCZ where motions are as strong as .35 cm/sec, rising. The correlation at 300 mbs (Fig. 52) seems to be the worst of all, but the channel two data for the area indicates that clouds only extend above 30,000 feet in parts of the southern ITCZ. Vertical velocities are of the order of .6 cm/sec. The magnitude of the vertical velocities for 3 March at all levels are considerably less than for the 1st.

Latent heat. The authors feel that the poor correlation with the ITCZ's at levels above 900 mbs is due to the lack of the latent heat contribution. Baumhefner (1966) has shown that the contribution from the latent heat forcing function easily runs as high as .5 cm/sec and could contribute more. These contributions to the upward motion would be found in areas with moisture convergence, R.H. > 60% and conditionally unstable conditions. These conditions would most likely be found in the areas of maximum cumulus cloud occurence which are right along our ITCZ's. Therefore, we feel that the addition of the latent heat team will bring the vertical velocities into a much closer correlation with the ITCZ's at levels above 900 mbs.

Inclusion of moisture for latent heat will be conducted this summer in a follow up study by Dr. T. N. Krishnamurti.

Friction. The higher correlation of the 900 mb level is believed to be due in large part to the effects of friction. Fig. 53 shows the contribution from the friction forcing function at the 900 mb level and it can be seen that there is an excellent correlation with the ITCZ's and that friction is a large contributor to the total vertical motion, running almost .4 cm/sec in some areas, which is over 40 percent of the total velocity. The authors would agree with Baumhefner that friction must be considered on a par with the forcing functions of the differential vorticity advection by the non-divergent wind and the Laplacian of thermal advection by the non-divergent part of the wind as the major contributors.

It might be mentioned that, initially, problems were encountered in computing friction at the 900 mb level and final friction contribution was not calculated until near the end of the research time period. As an alternative, in order to find the areas in which friction would have the most effect, a method to estimate the frictional vertical velocity at the top of the friction layer was utilized. This method is discussed by Panofsky (1956) and concerns the relationship of the frictional vertical velocity, through the Ekman Theory, to Equation (10).

$$w_H = \frac{\text{curl}\,\vec{\tau}_s}{\rho_H (\tilde{\beta} + f)} \qquad (10)$$

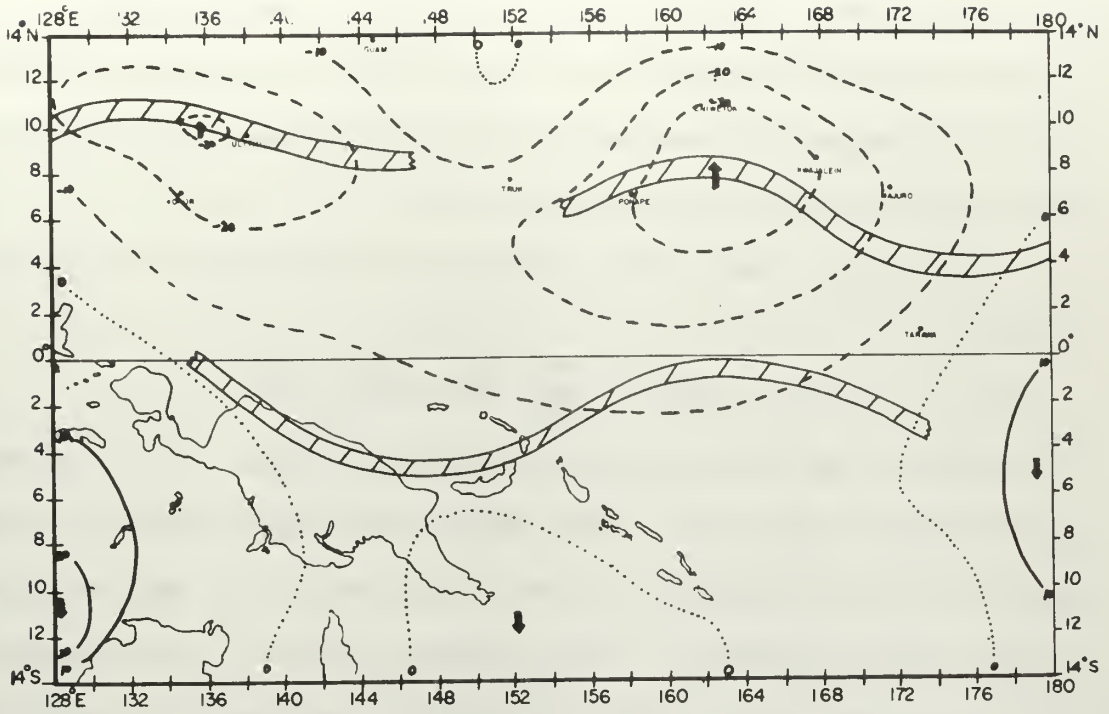

Fig. 53. Frictional component of vertical velocity at 900 mbs, 00Z 3 March 1965. ——— sinking, ····· neutral, ----- rising. ITCZ is cross-hatched. Interval, 10×10^{-5} mbs sec^{-1}.

Fig. 54. Relative vorticity (for computation of friction) at 1000 mbs, 00Z 3 March 1965. ——— anticyclonic vorticity, ----- cyclonic vorticity. Interval, 5×10^{-6} sec^{-1}.

Here, w_H is the vertical velocity produced by friction at the top of the friction layer, $\vec{\tau}_s$ is the surface stress, and $\bar{\zeta}$ denotes the average vorticity between the surface and the top of the friction layer.

Panofsky shows that this can be expressed in the simpler form

$$w_H = \frac{\mu_z}{2f\rho} \bar{\zeta}_{ogs} \sin 2\alpha_o . \qquad (11)$$

Here, μ_z is the eddy viscosity, $\bar{\zeta}_{ogs}$ is the surface geostrophic vorticity, and α_o is the angle between the surface wind and surface isobars. The quantity μ_z can also be eliminated by means of the relation between the height of the friction layer, H, and μ_z. The result is equation (12).

$$w_H = \frac{H}{\frac{3}{2}\pi + 2\alpha_o} \bar{\zeta}_{ogs} \sin 2\alpha_o . \qquad (12)$$

An estimate can be calculated for the frictional vertical velocity by subtracting the Coriolis parameter (f) from the absolute vorticity to obtain the relative vorticity (Fig. 54). This then can be used in Equation (12), along with a constant angle, α_o, over the ocean.

An example would be

$$\text{for } \zeta = 30 \times 10^{-6}/\text{sec}, \; H = 1 \text{ KM}, \text{ AND } \alpha_o = 30^\circ,$$

$$w_H = 0.35 \text{ cm/sec}$$

A comparison of Fig. 53 with Fig. 54 shows a high degree of correlation, if one remembers that negative values of ζ in the Southern Hemisphere represent cyclonic vorticity and we would have rising motions where they are located.

Other terms. Baumhefner (1966) found that in many instances the contributions of the vorticity advection and the Laplacian of thermal advection were of opposite sign. The same results were noted here, as illustrated by a comparison of the individual partial vertical velocities due to these forcing functions at 700 mbs (Figs. 55, 56).

The fact that the first two forcing functions, mentioned above, are generally the only major contributors to the vertical velocities above 900 mbs, in the absence of latent heat, is illustrated by a closer look at the 700 mb level. Fig. 57 shows the results if the sum of the contributions from vorticity advection and the Laplacian of thermal advection is subtracted from the total vertical velocity. It can be seen that the contribution of the sum of the remaining eight forcing functions that were calculated is almost negligible.

Vertical structure. A point along the northern ITCZ was selected for the 3rd of March, as was done for the 1st, to check the vertical structure of the magnitudes of the vertical velocities. The results at 8°N 144°E are shown in Fig. 58 and show the same basic structure as on the 1st. There are large values near the surface, due to friction, overlaid by small values at 700 mbs and larger values at higher levels before dropping off to zero at the top of the atmosphere.

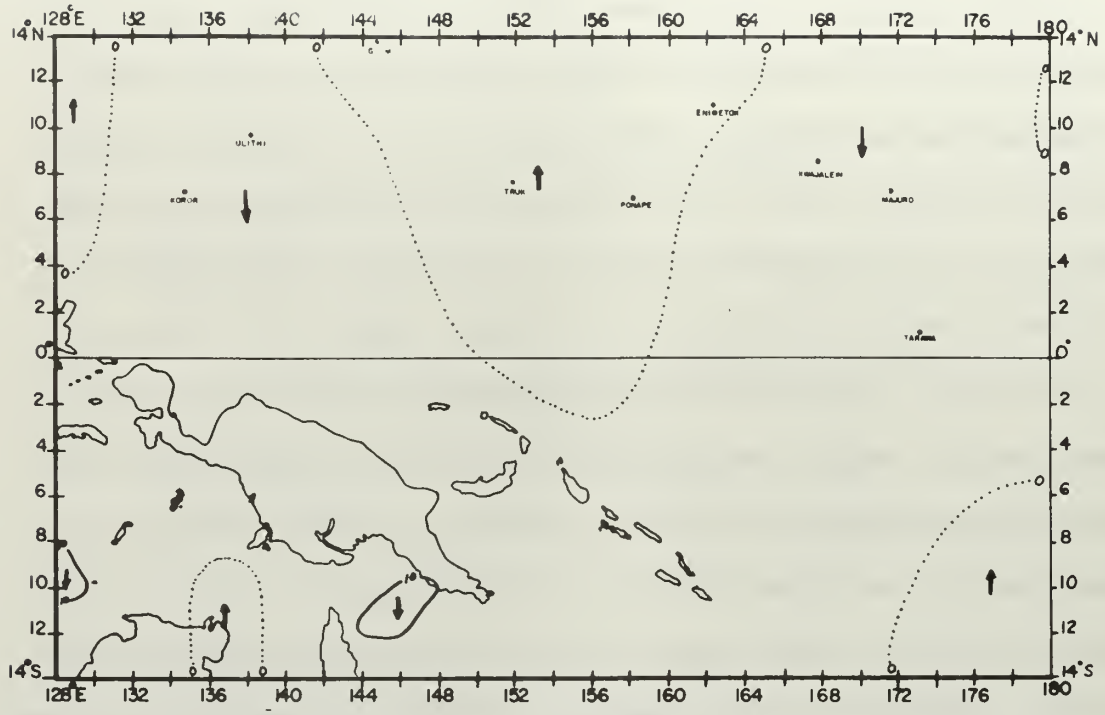

Fig. 55. Vertical velocity component due to differential vorticity advection by the non-divergent part of the wind, 700 mbs, 00Z 3 March 1965. ——— sinking, ····· neutral. Interval, 10×10^{-5} mbs sec^{-1}.

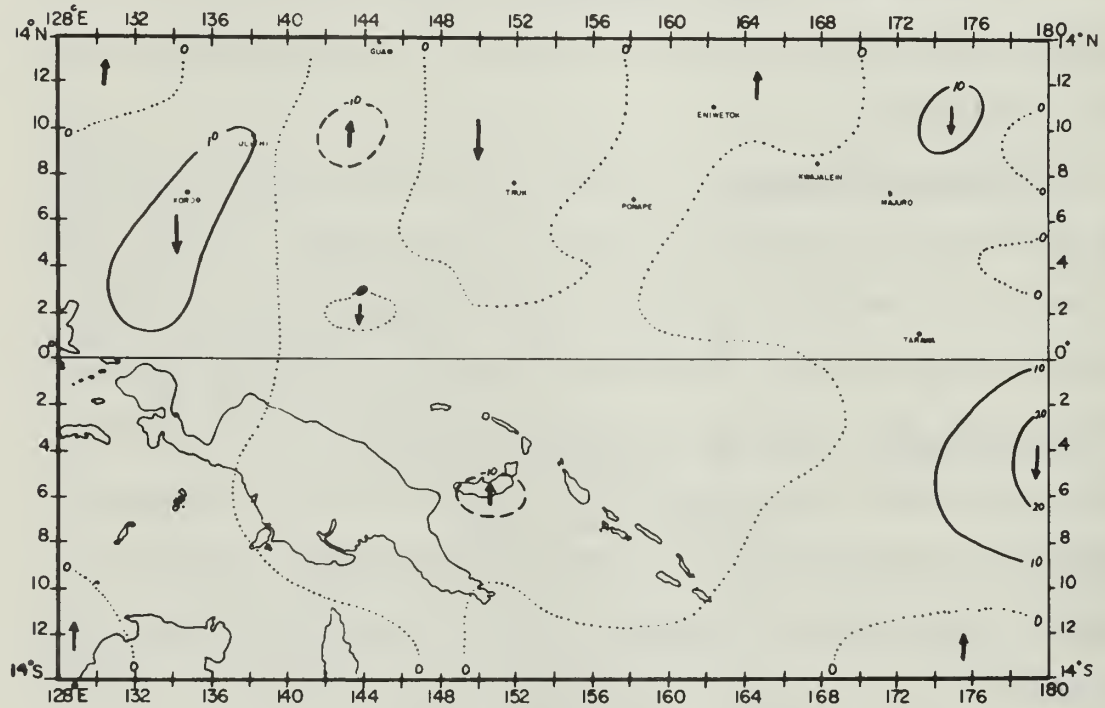

Fig. 56. Vertical velocity component due to the Laplacian of thermal advection by the non-divergent part of the wind, 700 mbs, 00Z 3 March 1965. ——— sinking, ····· neutral, ----- rising. Interval, 10×10^{-5} mbs sec^{-1}.

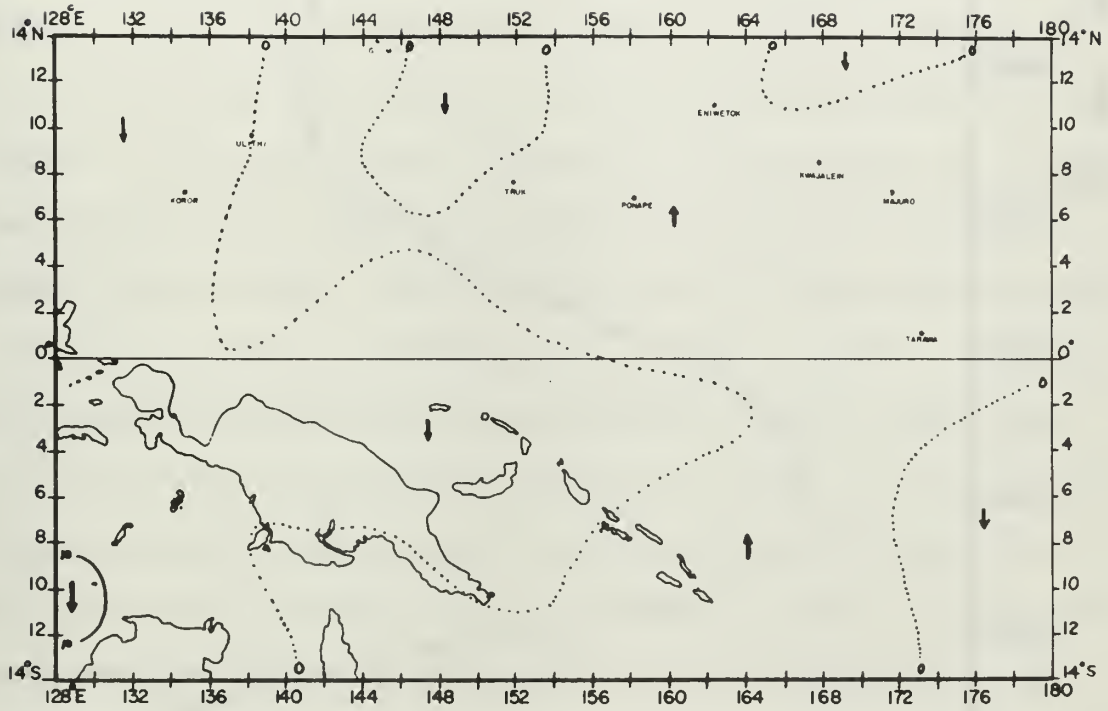

Fig. 57. Net contribution of vertical velocity from eight forcing functions after subtracting vorticity advection and Laplacian of thermal advection components from the total vertical velocity at 700 mbs, 00Z 3 March 1965. ——— sinking, ····· neutral. Interval, 10×10^{-5} mbs sec^{-1}.

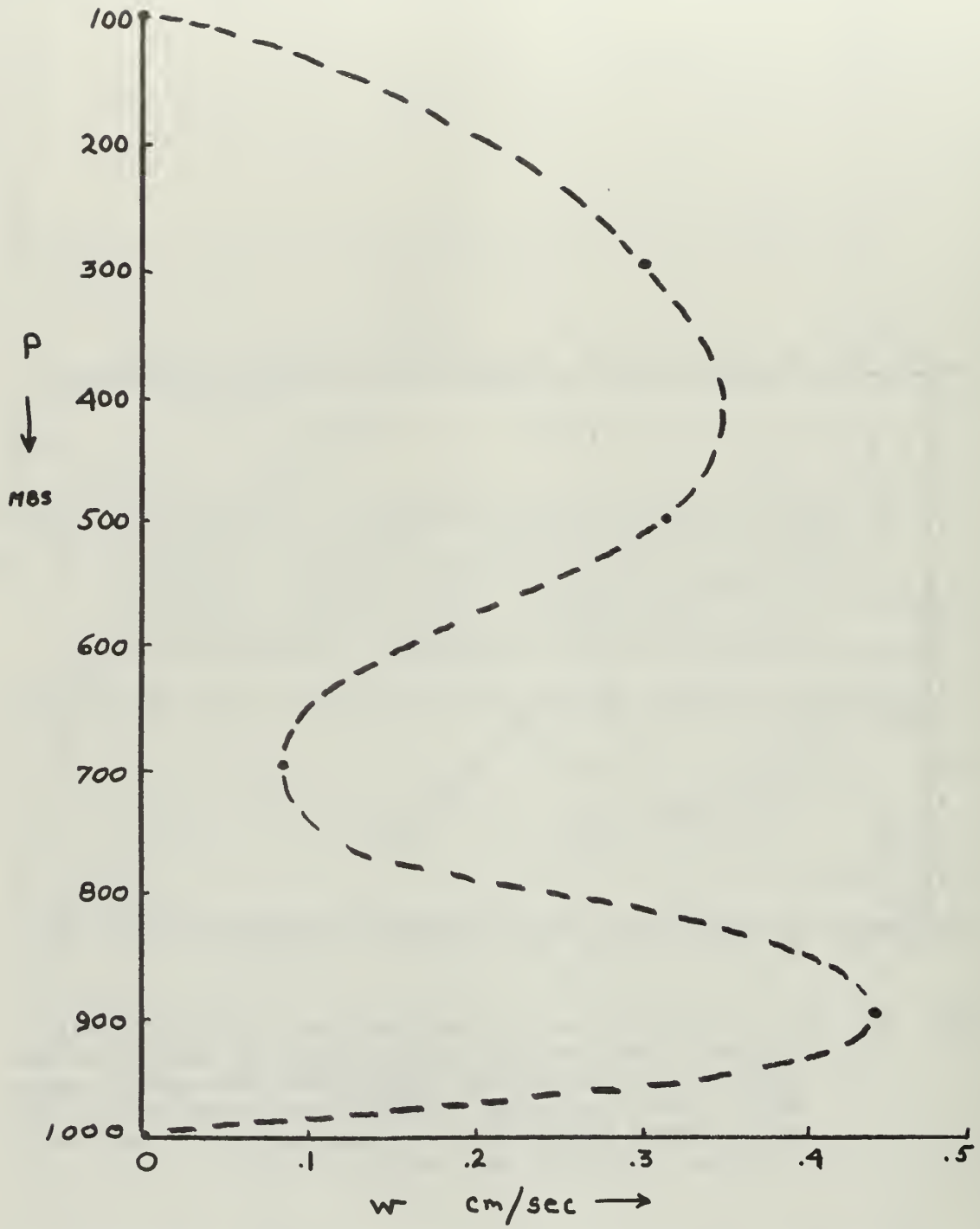

Fig. 58. Pressure versus vertical velocity (w) at 8°N 144°E, 00Z 3 March 1965.

V. CONCLUSIONS AND RECOMMENDATIONS FOR FURTHER STUDY

Several conclusions and recommendations are made based on the results of the study.

The relation between the calculated geopotential height fields and the stream fields becomes increasingly degraded with height, with the resemblance becoming negligible by 200 mbs. It appears that computation of the actual geopotential height field would be far superior in representativeness if this field were to be used in further calculations.

The close correlation of the non-divergent part of the wind to the actual wind illustrates the validity of current barotropic progs currently used by the weather bureau in Hawaii and by ESSA. These progs use just the non-divergent part of the wind at 500 mbs, from 30°N to 30°S. The non-divergent winds are obtained from the actual isogons and isotachs with calculations leading to $\nabla^2\psi$. The resulting winds are just moved ahead by prognosis. The results obtained by this method, since the non-divergent part of the wind represents about 90 percent of the actual wind, is probably better than what can be done by other methods until more complete information on winds and cloud coverage is available.

It is felt that the lack of a moisture input considerably degraded the correlations that might be expected between the vertical velocities and the ITCZ at levels above 900 mbs. Previous studies have shown that the latent heat term is a considerable contributor to the upward vertical

motion, especially in regions of extensive cumulus activity, such as the ITCZ. It is felt that the rising motion centers would have been more centrally located near the ITCZ's had the latent heat term been calculated. Further studies should definitely include this term in the tropics.

Two aids to the few dew point temperatures available for computing moisture are cloud pictures and the channel two water vapor data. Areas and types of cloud coverage may be obtained from cloud pictures and the channel two data is a good indication as to what level the clouds extend, thus being able to drop off the moisture content above that level. Krishnamurti has suggested an exponential decrease in moisture with height and this will be used in future studies as an alternate method of obtaining moisture. Nephanalyses appear to be too gross for use in numerical calculations and this is especially true in the tropics.

An illustration of the difficulties with the nephanalyses is the case of 1 March 1965. Fully 90 percent of the grid is covered by five-tenths or more clouds. Perhaps a more reliable interpretation of results can be obtained by selecting a day when photographs show a better defined, single ITCZ closer to its mean position for a particular season.

Terrain effects, although not included in this study, should be added in any region where significant land elevations occur. The effect of the high mountainous terrain of New Guinea could have made a significant difference in the final analysis.

The preliminary results of the vertical variation of ω at several points indicate that the tropical atmosphere may be characterized by large values of vertical motion near the surface, due to friction, small values at intermediate levels with much non-divergent flow and large values again at some higher level where the effect of a greater number of closed circulations is realized. The vertical motions are assumed zero at 100 mbs. This would indicate a vertical picture of strong inflow into a system near the surface with weak inflow or perhaps outflow near 700 mbs, inflow again above that level, and outflow near the top of the atmosphere. Further investigation into this subject is recommended.

It should be mentioned that a short range forecast is being made for this area in the future, utilizing the results obtained here, in a primitive equation prediction model. This is being done in a manner correct for small Rossby number by Dr. T. N. Krishnamurti.

Further observational work, both through the use of conventional data and through the use of satellite cloud photography and infrared radiometric probes will undoubtedly provide better grounds for parameterization of the sub-grid scale phenomenon, and continue to give us a better understanding of the tropical atmosphere.

VI. BIBLIOGRAPHY

1. Baumhefner, D. P. "The Dynamical Structure of the Tropical Atmosphere Based on Experiments with a Diagnostic Numerical Model." Unpublished Master's thesis, Department of Meteorology, University of California, Los Angeles, 1966. 165 pp.

2. Charney, J. G. "The Use of the Primitive Equations of Motion in Numerical Weather Prediction," Tellus, Vol. 7, 1955, pp. 22-26.

3. _____. "Integrations of the Primitive and Balance Equations," Proceedings of the International Symposium on Numerical Weather Prediction, pp. 131-152. Tokyo, Japan: The Meteorological Society of Japan, 1962.

4. _____. "A Note on the Large Scale Motion in the Tropics," Journal of Atmospheric Sciences, Vol. 20, 1963, pp. 607-609.

5. Hawkins, H. F., and S. L. Rosenthal. "On the Computation of Stream Functions From the Wind Field," Monthly Weather Review, Vol. 93, No. 4, 1965, pp. 245-252.

6. Krishnamurti, T. N. "Numerical Studies of Organized Circulation in Subtropical Latitudes." Scientific Report (CWB 10877), Environmental Science Services Administration, 1966a. 90 pp.

7. _____. "A Diagnostic Balance Model for Studies of Weather Systems of Low and High Latitudes (Rossby Number < 1)," Final Report to AFCRL, Air Force Cambridge Research Laboratories, Bedford, Mass., 1966b. 42 pp.

8. _____, J. Nogues, and D. P. Baumhefner. "On the Partitioning of the Baroclinic Vertical Motions in a Developing Wave Cyclone," Scientific Report (AFCRL 66-419), Air Force Cambridge Research Laboratories, Bedford, Mass., 1966. 59 pp.

9. Kuo, H. L. "On Formation and Intensification of Tropical Cyclones Through Latent Heat Release by Cumulus Convection," Journal of Atmospheric Sciences, Vol. 22, 1965, pp. 40-63.

10. Miyakoda, K. "Some Characteristic Features of Winter Time Circulations in the Troposphere and Lower Stratosphere," Technical Report No. 14, University of Chicago, 1963.

11. Ooyama, K. "A Dynamical Model for the Study of Tropical Cyclone Development." Unpublished Scientific Report, Department of Meteorology and Oceanography, New York University

12. Palmer, C.E. "Tropical Meteorology," Compendium of Meteorology. American Meteorological Society, Boston, Mass., 1951, pp. 859-917.

13. Panofsky, H. Introduction to Dynamic Meteorology. Pennsylvania: Pennsylvania State University, 1956. 243 pp.

14. Riehl, H. Tropical Meteorology. New York: The McGraw Hill Book Company, 1954. 392 pp.

15. _____, and J. S. Malkus. "On the Heat Balance in the Equatorial Trough Zone," Geophysica, Vol. 6, 1958, pp. 503-525.

16. Rosenthal, S. L. "Some Attempts to Simulate the Development of Tropical Cyclones by Numerical Methods," Monthly Weather Review, Vol. 92, 1964, pp. 1-21.

17. Roth, H. S., D. W. Rabenhorst, and T. A. Stanbury. "Intertropical Convergence Zone Meteorology." Scientific Report (NORD 7386), Bureau of Ordnance, Department of the Navy, 1958.

18. Thompson, P. D. Numerical Weather Analysis and Prediction, New York: The Macmillan Company, 1961.

19. Wiederanders, C. J. "Analyses of Monthly Mean Resultant Winds for Standard Pressure Levels Over the Pacific." Scientific Report (AFCRL 296) Air Force Cambridge Research Laboratories, Bedford, Mass., and Navy Weather Research Facility, Norfolk, Va., 1961. 83 pp.

20. U.S. Department of Commerce, Environmental Science Services Administration. Catalogue of Meteorological Satellite Data - Tiros IX Television Cloud Photography. Washington: Government Printing Office, 1966.

INITIAL DISTRIBUTION LIST

		No. Copies
1.	LT John F. Murray, USN 825 E. Haines St. Philadelphia, Pennsylvania	1
2.	LCDR Phil G. Prokop, USN U.S. Fleet Weather Facility U.S. Naval Station FPO New York, N.Y. 09571	1
3.	Prof T. N. Krishnamurti Department of Meteorology & Oceanography Naval Postgraduate School Monterey, California 93940	5
4.	Library Naval Postgraduate School Monterey, California 93940	2
5.	Officer in Charge Naval Weather Research Facility Naval Air Station, Building R-48 Norfolk, Virginia 23511	1
6.	Commanding Officer U.S. Fleet Weather Central Box 12, COMNAVMARIANAS FPO San Francisco, California 96601	1
7.	Commanding Officer U.S. Fleet Weather Central Box 10 FPO San Francisco, California 96610	1
8.	Officer in Charge U.S. Fleet Weather Facility FPO New York, New York 09571	1
9.	Officer in Charge U.S. Fleet Weather Facility FPO San Francisco, California 96652	1
10.	Officer in Charge Fleet Weather Facility P.O. Box 85 Naval Air Station Jacksonville, Florida 32212	1

		No. Copies
11.	Officer in Charge Fleet Numerical Weather Facility Naval Postgraduate School Monterey, California 93940 Attn: Mr. Leo Clarke	2
12.	Director, Naval Research Laboratory Attn: Tech. Services Info. Officer Washington, D. C. 20390	1
13.	AFCRL - Research Library L. G. Hanscom Field Attn: Nancy Davis/Stop 29 Bedford, Massachusetts 01730	1
14.	Dept. of Meteorology & Oceanography Naval Postgraduate School Monterey, California 93940	3
15.	Defense Documentation Center Cameron Station Alexandria, Virginia 22314	20
16.	Office of the Naval Weather Service Naval Station (Washington Navy Yard Annex) Washington, D. C. 20390	1
17.	Commander, Air Weather Service Military Airlift Command U.S. Air Force Scott Air Force Base, Illinois 62226	2
18.	Department of Commerce, ESSA Weather Bureau Washington, D. C. 20235	2
19.	LCDR J. D. Jarrell Naval Weather Research Facility Naval Air Station, Building R-48 Norfolk, Virginia 23511	1

DOCUMENT CONTROL DATA - R&D

(Security classification of title, body of abstract and indexing annotation must be entered when the overall report is classified)

1. ORIGINATING ACTIVITY (Corporate author)	2a. REPORT SECURITY CLASSIFICATION
Naval Postgraduate School Monterey, California	UNCLASSIFIED
	2b. GROUP

3. REPORT TITLE

The Intertropical Convergence Zone and Vertical Motions Using a Diagnostic Numerical Model

4. DESCRIPTIVE NOTES (Type of report and inclusive dates)

5. AUTHOR(S) (Last name, first name, initial)

Prokop, Phil G., LCDR, USN
Murray, John F., LT, USN

6. REPORT DATE	7a. TOTAL NO. OF PAGES	7b. NO. OF REFS
June 1967	86	20

8a. CONTRACT OR GRANT NO.	9a. ORIGINATOR'S REPORT NUMBER(S)
b. PROJECT NO.	
c.	9b. OTHER REPORT NO(S) (Any other numbers that may be assigned this report)
d.	

10. AVAILABILITY/LIMITATION NOTICES

[redacted]

11. SUPPLEMENTARY NOTES	12. SPONSORING MILITARY ACTIVITY

13. ABSTRACT

A diagnostic, non-linear balanced model is applied to a case study in the tropical Western Pacific on 1 and 3 March 1965. The region includes both sides of the equator and contains the ITCZ.

A discussion of the ITCZ is given and the model is discussed along with the processing of the input data. The study contains the horizontal wind velocity and the thermal distribution as input values. The non-divergent stream function (Ψ) is obtained by relaxation of the Poisson Equation, $\nabla^2\Psi = k\cdot\nabla\times V = \zeta$, where the vorticity is computed from the observed wind field. A comparison is made between the non-divergent part of the wind and the actual wind. Computer analyzed stream functions at several levels are shown and discussed.

Dry adiabatic vertical velocities are obtained and compared with the ITCZ. Typical magnitudes are on the order of 0.5 cm/sec. The forcing functions of the ω equation are shown and the contributions, in partitioned form, by various terms are illustrated and discussed at several levels.

14. KEY WORDS	LINK A		LINK B		LINK C	
	ROLE	WT	ROLE	WT	ROLE	WT
Intertropical Convergence Zone						
Diagnostic						
Non-linear						
Balanced Model						
Non-divergent						
Stream function						
Partitioned						
Vertical motion						